Highly Efficient Dye Sensitized Solar Cells with Integrated 3D Graphene-Based Materials

Hisham A. Maddah[a,b], Anmole Jhally[a], Vikas Berry[a], Sanjay K. Behura[a*]

[a] Department of Chemical Engineering, University of Illinois at Chicago, 945 W Taylor St, Chicago, IL 60607, United States

[b] Department of Chemical Engineering, King Abdulaziz University, Rabigh 21911, Saudi Arabia

*corresponding email address: sbehura1@uic.edu

ABSTRACT

Dye-sensitized solar cells (DSSCs) have gained broad interest as a promising low cost third-generation technology with decent power conversion efficiency (PCE). Efficient DSSCs demand maximum photon absorption and minimum electron-hole recombination; achieved from using various photoanode and cathode architectures. Graphene and 3D graphene-based materials (3D-GBMs) have been recently explored to be incorporated in DSSCs for photocurrent enhancements. Highly porous structure and interconnected pore networks/channels in 3D-GBMs provide excellent electrical conductivity, large specific surface area, and high electrocatalytic activity supporting rapid electron transport in 3D space. 3D-GBMs are synthesized by: (i) self-assembly approaches and/or (ii) template-directed approaches. A few reports demonstrated the promise behind integrating 3D-GBMs into DSSCs: (i) 3D/2D [3D-GBMs with reduced graphene oxide (rGO)] counter electrodes (CEs) achieved a PCE of 9.79%, (ii) [PDDA@ERGO] CEs are highly efficient (9.5%) and durable for long-time operation, (iii) 3D-GBMs/1D-ZnO photoanodes enhanced electrolyte reduction for high J_{sc} and PCE (8.12%), and (iv) rGO–TiO_2 photoanodes achieved high PCE (5.83%) with 0.5 mg rGO. Finally, the use of toxic-free carotenoids/proteins sensitizers has been highlighted for enhanced photoanode visible-light absorption. In conclusion, engineered electrode architectures based on 3D-GBMs foster the overall device PCE owing to the introduced extra electron pathways and reduced charge resistance.

Table of Contents

9.1 Introduction

Sun radiation provides earth with abundant, free, and environmental-friendly solar energy with power of approximately 1.8×10^{11} MW[1]. Harnessing solar power *via* photovoltaics (PV) allows us to efficiently convert incident photons to excitons for electricity generation[1]. Nevertheless, efficient first-generation silicon-based solar cells are expensive and can be potentially replaced by cost-effective alternatives as second-generation multi-crystalline Si[2–6] or third-generation PV systems including organic/inorganic perovskits[7–15], cadmium telluride (CdTe), copper indium gallium selenide (CIGS)[16–23], organic tandem[24–30], quantum dot cells[31–36], and dye-sensitized solar cells (DSSCs)[37–47].

Among all the third-generation photovoltaic systems, DSSCs have taken up broad interest as a promising low cost solar cell technology. Sensitized solar cells use specialized materials for specific cell functions including photon absorption, charge separation, and charge transport. A photon enters the solar cell through a transparent electrode and can be absorbed by a sensitizer, thus exciting an electron. This electron can be injected into the conduction band of a neighbouring semiconductor and diffuse. The diffused electron can perform work, given to an external load, and flow to the cathode where it is transferred to an electrolyte or a hole conductor. The electrolyte can then transfer an electron to the sensitizer, regenerating it and completing the circuit. To optimize these devices and achieve respectable power conversion efficiencies (PCEs), researchers have looked at ways to maximize light harvesting and minimize electron losses due to parasitic electron transfer pathways[48].

To date, a significant progress has been made towards the development of DSSCs through: (i) material selection, (ii) architecture of photoanode wide bandgap semiconductors (e.g. TiO_2, ZnO, SnO_2, TiO_2/ZnO, SnO_2/ZnO, ZnO/SnO_2, SnO_2/TiO_2, TiO_2/ZnO/TiO_2), (iii) counter electrodes (e.g. C, Pt, C/Pt, GQDs), and (iv) electrolyte selection in either liquid-state (e.g. iodide/triiodide redox) or solid-state (e.g. cobalt complexes). The incorporation of graphene and 3D graphene-based materials (3D-GBMs) in DSSCs as electrodes show a potential for further improvement of photovoltaic conversion. Moreover, the use of toxic-free natural sensitizers (e.g. β-Carotene) extracted from carotenoids and protein complexes[49] and/or perovskite semiconductors (for cosensitization) hold the promise to enhance visible-light absorption in DSSCs, instead of using the very toxic and expensive[50] commercial dyes including organic dyes,[43] ruthenium dyes[51], and platinum dyes[52].

DSSCs can become more efficient from incorporation of graphene sheets. Graphene materials (e.g., CVD graphene and rGO) have been studied as transparent conductors, in the semiconducting layer, and even as the sensitizer itself for the photoanode of a DSSC. Furthermore, graphene sheets have been used to optimize the efficiency of nearly every main component of a DSSC, which can improve the overall performance and/or reduce the cost of such devices[53]. 3D-Graphene/TiO_2 nanocomposites are appropriate photoanodes for DSSCs owing to the 3D-GBMs high [transparency, electron transfer mobility, and electrochemical activities], which also makes 3D-GBMs perfect for counter electrode applications[54]. The combination of the excellent graphene electrical conductivity and the large surface area (from porous and interconnected networks) make 3D-GBMs a promising anode/cathode material for building DSSCs with enhanced photovoltaic properties and superior performance[55].

9.1.1. Dye-Sensitized Solar Cells

The idea of DSSCs was initiated in 1991 by O'Regan and Grätzel[37] inspired by natural photosynthesis and photography processes[56]. Molecular pigments found in plants and fruits absorb visible-light energy to excite free electrons residing in conjugated-bond structures. DSSCs convert solar energy into electrical energy *via* a pigmented thin-film semiconductor material that absorbs photons for excitons generation[37]. Since 1991, DSSCs PCE has improved from 7.1% to 13% (2014) from involvement of different Ru-based sensitizers and photoanode or cathode structures[57]. Cosensitization of TiO_2-solid-state DSSCs with perovskite semiconductors ($CH_3NH_3PbX_3$) found also to be promising for increasing the cell performance up to 15%[58]. Electricity production costs in DSSCs are below \$0.5/W, owing to their inexpensive materials and components, whereas silicon solar cells costs around \$2.7–3.57/W[1,40,59,60]. This gives a great advantage for DSSCs systems to be utilized as

potential photovoltaic molecular machines sensitizing a wide-bandgap semiconductor (e.g. TiO_2, ZnO, and SnO_2) photoanode for electron excitation, injection, and current generation[56]. Large surface area nanoporous semiconductors can absorb pigments and create a monolayer of dye molecules generating electron-hole pairs upon visible-light illumination; charge separation occurs in femtoseconds at the semiconductor/dye interface resulting in the injection of an electron from the dye molecules into the conduction band of the semiconductor[41,61].

9.1.2. Architecture and Working Mechanism

Conventional DSSCs consist of four main components: (i) photoanode, (ii) photosensitizer, (iii) electrolyte, and (iv) counter electrode (cathode)[60]. The four components works synergistically to convert visible sunlight energy into electricity (photons-to-electrons) starting from the photosensitizers being sensitized for electron excitation/injection[56,59,60,62–64]. Typical materials of the key components and their role in electron excitation and transportation are shown in Table 1; giving us the opportunity to understand charge transfer mechanisms for PCE enhancement. Low sheet resistance (15 to 40 Ω/■) of transparent conductive oxide (TCO) glass sheets [as indium-doped tin oxide (ITO) or fluorine-doped tin oxide (FTO)] is desired to allow easy electron transport from TiO_2 to ITO and thereby to the counter electrode for current generation. High optical transmittance of ITO (>85%) for visible-light (400 to 700 nm) makes it a promising candidate for the photoanode architecture in DSSCs. Moreover, utilization of thin-film semiconductors, fabricated from crystallization and annealing of TiO_2 nanoparticles at 100 and 500 °C, is critically important to reduce series and/or interfacial charge resistance facilitating charge transfer and conduction. Covalently bonded monolayer dye molecules onto the semiconductor exposed surface (nanoparticles) would improve photons absorption and electron-hole pair generation

under standard solar illumination (AM1.5). Using a charge transport medium (redox electrolyte) applied between the two electrodes is necessary for uninterrupted electron transport and dye neutralization. Liquid or solid (gel) electrolytes regenerate missing electrons of the oxidized dye molecules by donating the received electrons from the cathode electrode (i.e. oxidation/reduction of iodide and triiodide $[I^-/I_3^-]$ redox couple)[56,59,60,62–67]. A schematic representation of a typical DSSC system with its main components is shown in Figure 1.

Table 1. Components of a Typical DSSC: Key components and their roles in electron excitation, separation, transportation, and current generation.

S/N	Component	Typical DSSC	Role in Charge Generation and Transfer
i	Photoanode electrode	ITO/TiO_2/Dye	Charge conduction of received dye electrons and charge separation/transport at TiO_2/Dye.
ii	Counter electrode	ITO/Pt (or) ITO/C	Electron collection of photoanode electrons.
iii	Photosensitizer (part of the photoanode)	Commercial metal Ru-dyes (e.g. N3, N719, and N749)	Electron excitation, injection, and charge transfer to the semiconductor.
iv	Redox electrolyte	$[I^-/I_3^-]$ redox couple	Dye regeneration by reduction/oxidation.

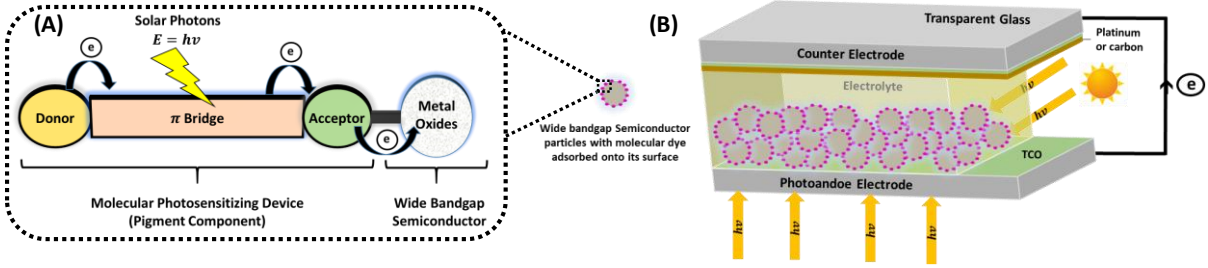

Figure 1. Schematic Representation of a Typical DSSC: (A) Donor-π-acceptor (D-π-A) structure of an organic dye in DSSCs with a wide bandgap semiconductor photoanode; **(B)** Typical components and architecture including photosensitizer for electron injection, photoanode electrode for charge separation/transport, counter electrode for electron collection, and redox electrolyte for dye neutralization, from[67].

To understand how current is being generated within DSSCs, the working mechanism, operation cycle and electron transport from visible-light excitation can be summarized as[56,60,62,65,66]:

a) Dye excitation: Absorption of incident photons energy will excite dye molecules from their ground state (S) to a higher energy state (S*); this is equivalent to movement of dye electrons from their highest occupied molecular orbital (HOMO) to their lowest unoccupied molecular orbital (LUMO) in the dye organic molecular structure forming electron-hole pairs.

b) Electron injection: Once a dye electron is excited (S*), an electron from S* transports from the dye acceptor segments (in the D-π-A structure) and is injected into the conduction band of the semiconductor (e.g. TiO_2); the electron injection ensures charge separation and allows continuously generated electrons to flow through the photoanode structure towards the cathode charging an external load in every completed cycle.

c) Oxidized-Dye regeneration: An electron donation from iodide (I_3^-) in the redox electrolyte [I^-/I_3^-] will regenerate oxidized-dye (S^+) for repeatable electron excitation/injection.

d) Electrochemical reduction: At the cathode side, transported photoanode electrons collection occurs while the redox mediator gets regenerated from reduction of triiodide ($3I^-$).

9.1.3. Electron Transport and Recombination Kinetics

To facilitate electron transport in DSSCs, electron recombination with either oxidized dye molecules (e1) or electrolyte species (e2) should be reduced[65,66]. The timescale of electron transfer at the interfacial contacts determines the controlling recombination

reactions[68]. Typically, photogenerated electrons recombine within 10 μs[69,70], where the electron transfer occurs within 10 fs and 1 ns at the semiconductor/dye and dye/electrolyte interfaces, respectively. Due to the faster electron injection rates, recombination dynamics in DSSCs are believed to be controlled by the slow transport of reduced electrolyte electrons[65]. The discussed operation cycle and mechanisms of electron transport in DSSCs with typical reactions at anode, cell, and cathode and expected recombination are illustrated in Figure 2(A–C).

If an excited electron is lost across the semiconductor/dye interface, the electron follows the (e1) path and recombines with available holes in the oxidized dye molecules under visible-light illumination. However, lost electrons across the dye/electrolyte interface follow (e2) path and recombine with available holes in the oxidized redox electrolyte under dark current situations and/or no visible-light illumination. Recombination occurs at the phase contacts when electrons are being transferred from ITO to electrolyte, electrolyte to dye, dye to the semiconductor (TiO_2), TiO_2 to ITO, and so on. Most importantly, recombination dynamics at the TiO_2/electrolyte and the TiO_2/dye interfaces, as shown in Figure 2(A) and Figure 2(E), are very common and crucial to control for enhanced electron excitation/injection[63,65,71,72]. There should be a reasonable back electron transfer blockage from the semiconductor, where injected electrons from dye acceptor segments must remain in the semiconductor with exclusively forward transport required for reducing recombination rates and facilitating electron injection. Huge surface area exists in TiO_2 films interfaced with dyes containing many hydroxyl and carboxyl anchoring groups provide efficient charge injection and forward electron transfer at the TiO_2/dye and TiO_2/ITO interfaces[65,73].

There is always a competition between recombination and regeneration reactions arising from oxidation/reduction of both dye molecules and electrolyte redox species. Further, possible recombination reactions compete with each other where lost electrons are either drifted back to recombine with oxidized dye molecules or oxidized redox species in the electrolyte[66].

Moreover, it has been discussed that electron lifetime can be tuned by changing the deposited dye amounts onto the photoanode structure. Slight increases in the organic dye amounts may result in prominent enhancement in generated electron lifetimes, yielding in lowered recombination rates and improved photocurrents. Ruthenium metal-based dyes utilized in DSSCs show high photocurrent and decent V_{oc} from less electron recombination at the dye/electrolyte or dye/semiconductor interfaces, due to lots of available carboxyl groups. Conversely, organic pigments extracted from natural sources such as plants, carotenoids, and protein complexes show excess interfacial electron recombination and low photocurrents[74,75], which may be improved by the incorporation of 3D-GBMs in the anode structure. Another approach to mitigate interfacial recombination at the photoanode interfaces include photoanode passivation or insulation using SiO_2, Al_2O_3, and ZrO_2 layers, which would create a metal-oxide barrier preventing back electron transport to the electrolyte[63,76].

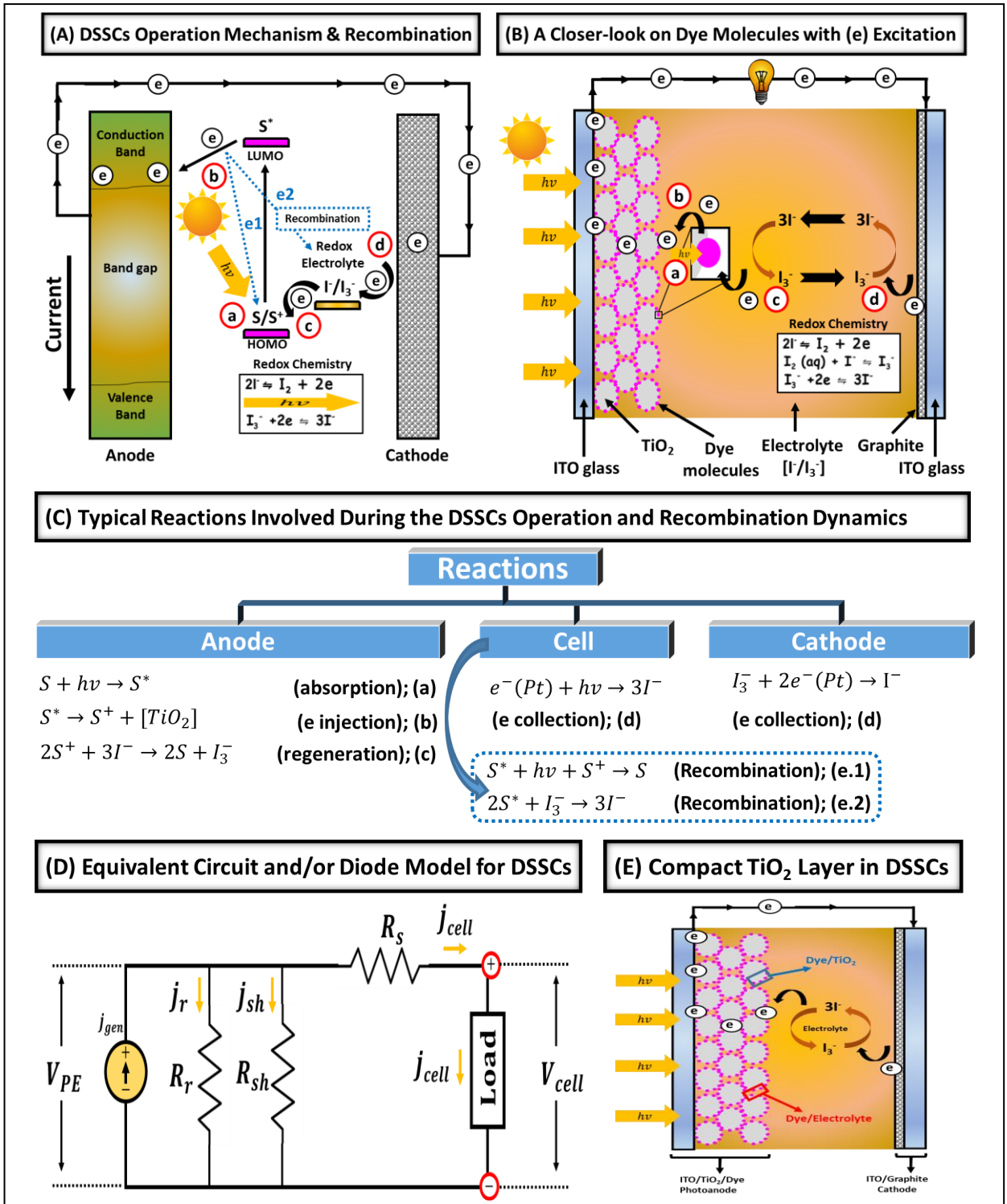

Figure 2. DSSC Operation Cycle and Reactions: (A) DSSCs complete operation cycle and recombination dynamics; **(B)** Closer-look on the electron excitation and transport in DSSCs; **(C)** Anode (TiO_2) and cathode (Pt/C) typical redox reactions in a DSSC (electron flow depends on light intensity and trapping-detrapping effect of the surface); Charge regeneration mechanism in (A) and (B): (a) photons energy excite electrons from HOMO to LUMO levels and generate excitons within the dye molecules to (b) inject excited electrons into the conduction band of the semiconductor which initiate charge separation/transport of electrons from photoanode electrode to cathode electrode for current generation while (c) electrolyte ensures continuous current generation by neutralizing dye molecules through (d) redox reactions mechanism, with (e1) and (e2) describing possible recombination within DSSCs; **(D)** Diode model for DSSCs; **(E)** TiO_2 photoanode compact layer in DSSCs, from[67].

9.2 Graphene and 3D Graphene-Based Materials (3D-GBMs)

Pristine graphene is an atomic layer of sp^2-hybridized carbon arranged in a honeycomb structure[48]. Graphene-based materials, with their exceptional electrical, optical, and mechanical properties, have been previously incorporated into each aspect of a DSSC[48]. Interestingly enough, this amazing material can be derived from graphite (*via* top-down approach), which is economical and naturally abundant[77]. Wang et al. (2012)[78] utilized graphene-based composites in DSSCs owing to its excellent conductivity and high electrocatalytic activity. The hexagonal "honeycomb" two-dimensional sp^2 carbon atoms[79] possesses high carrier mobility (200,000 $cm^2\ V^{-1}\ s^{-1}$)[80], high specific surface area (2600 $m^2\ g^{-1}$)[81], and high optical transparency (97.7%)[82]; making graphene a promising material to be utilized as electrodes for efficient and practical DSSCs. Besides the discussed 2D graphene properties, 3D-GBMs (e.g. aerogels, hydrogels, sponges) are characterized with interconnected networks/channels providing large specific surface area, high electrochemical stability, and excellent mechanical strength[83].

9.2.1. Synthesis Methods

Graphene sheets have been typically produced either by mechanical exfoliation *via* repeated peeling of highly ordered pyrolytic graphite (HOPG) or by chemical oxidation of graphite (top-down approach)[84]. In the past few years, a number of approaches have been established to fabricate 3D interconnected structures of graphene (e.g., ice template, wet chemistry assembly, self-gelation, freeze casting, chemical vapor deposition (CVD), and *in situ* unzipping of carbon nanotubes sponge) (Min et al., 2013; Fang et al., 2015). For most of the methods, freeze-drying or supercritical drying is essential to inhibit capillary-force-driven structural collapse of graphene 3D networks

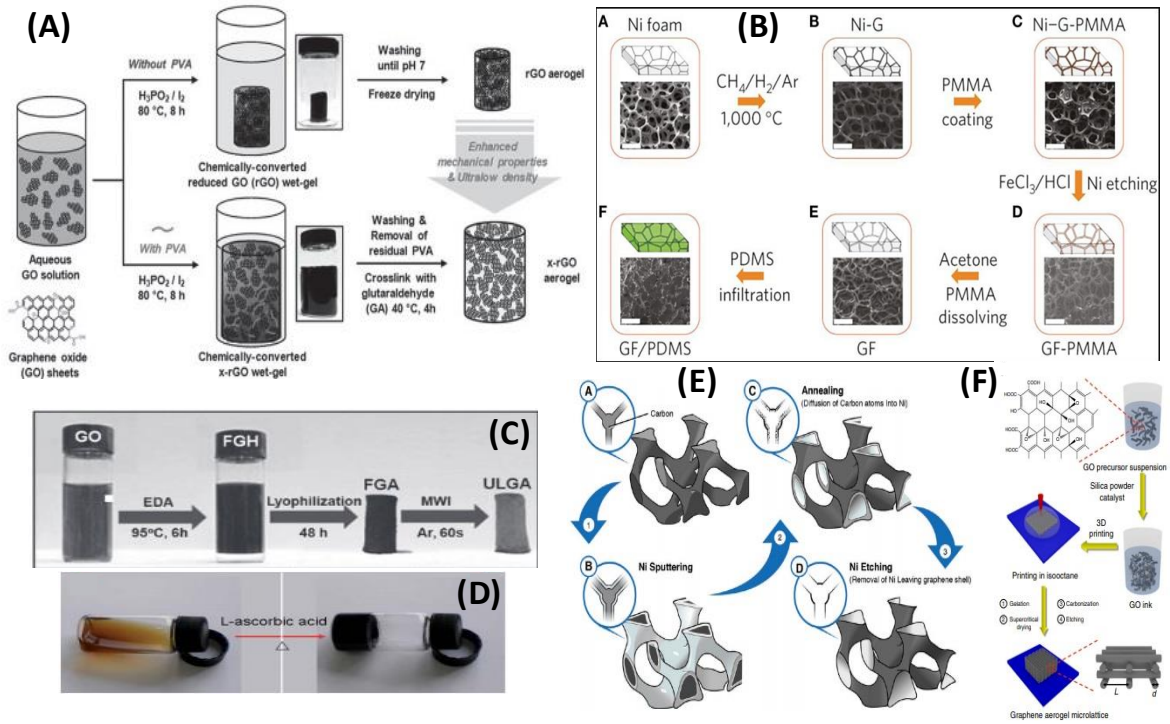

Figure 3. (A) Schematic illustration of the different steps for fabricating reduced graphene oxide (rGO) aerogel, from[95]; **(B)** Synthesis of a graphene foam (GF) and CVD growth of graphene films (Ni–G) integrated with PDMS, from[87]; **(C)** Illustration of the fabrication process of ultralight graphene aerogel (ULGA), from[93]; **(D)** Aqueous suspension of graphene oxide (GO) hydrogel to graphene aerogel before and after heating and mixing with L-ascorbic acid and freeze-drying, from[94]; **(E)** illustration for the mechanism of chemical conversion of amorphous porous carbon to 3D graphene, from[91]; **(F)** Schematic of the fabrication process for graphene aerogel from mixing GO suspension with silica powders and R–F catalyst forming GO ink templated on SiO_2, from[90].

during drying[85]. The synthesis of 3D-GBMs mainly start from using precursors of graphene oxide (GO) following either of the two mechanisms, discussed in literature, including self-assembly approaches and template-directed approaches[86–95], resulting in 3D graphene architectures with different structures and properties. Bai et al. reported that 3D assembly of GO sheets in water is possible by adding polyvinyl alcohol (PVA) as a cross-linker, forming a pH-sensitive supramolecular hydrogel. Hydrogen bonding between GO sheets and PVA chains is believed to be responsible for the formation of the hydrogel[96]. Recently, single-stranded DNA was also found to be a good cross-linker for preparing GO/DNA composite hydrogel, in which π-π interaction was the dominant driving force[97]. Similarly, hydrogels based on chemically

254 concerted graphene (CCG) have also been reported reflecting that GO and CCG are
255 good gelators. The GO-based hydrogels were prepared by acidification or adding
256 small organic molecules, polymers, or ions as cross-linkers[96].

257 **Table 2.** Synthesis Methods for 3D-GBMs *via* template directed approach (1 to 5) or
258 assisted/induced self-assembly mechanism (6 to 10).

S/N	Method	Experiment	Ref.
1	CVD Approach	Nickel foams are heated and annealed, then a thin PMMA layer is used. Next, Nickel/PMMA is baked and dissolved in hot acetone bath to obtain free-standing graphene foams (GFs).	87
2	Ice Template	Graphene oxide (GO) solution is mixed with ascorbic acid, then placed in boiling water bath. Next, the solution is immersed in a dry ice bath to freeze, then thawed at room temperature. The obtained gel is then sequentially subjected to dialysis in water, freeze-drying, and thermal annealing.	88
3	Emulsion Template	GO is prepared and organic additives are added. Next, the aqueous nanocarbon suspensions are emulsified with a hydrophobic phase. The nanocarbon emulsion is unidirectionally frozen and bulk nanocarbon monoliths are obtained by freeze-drying. The nanocarbon monoliths are thermally reduced to produce the final reduced GO (rGO) monoliths.	89
4	SiO_2 Template	GO powder is produced then gelled into GO ink. The sol–gel mixture consists of an aqueous solution of resorcinol (R), formaldehyde (F) and sodium carbonate catalyst (C). 3D periodic micro lattices were assembled by patterning an array of parallel (rod-like) filaments in a meander line-like pattern. After gelation, the wet GO gels are removed, washed, and dried.	90
5	Lithographical Template	A bottom antireflection coating is spun onto silicon wafers and baked. A thin resist layer of NR 7 is deposited and a thick resist layer (6 μm) of NR7-6000P is deposited. An interference pattern is formed, and the beam is expanded and split. Finally, the samples are baked and rinsed.	91
6	Hydrothermal Reduction	A suspension of GO is prepared by sonication involving a noble-metal salt and glucose. The mixture is then treated hydrothermally, washed, then freeze-dried.	92
7	Cross Linking Agent	GO dispersion is mixed uniformly with ethylenediamine and freeze-dried. After freeze-drying, functionalized graphene aerogel (FGA) is produced and exposed to microwave irradiation (MWI). The MWI restores interaction in the cross-linking sites, which tightly bonds the sheets together.	93

8	Reducing Agent	Heating the aqueous mixture of GO with L-ascorbic acid without stirring.	94
9	Polymer Assembly	Aqueous GO solution is prepared then freeze-dried into rGO aerogel. Next, PVA is dissolved then Hypophosphorous acid and Iodine are added. The suspension undergone reaction, then washed and treated with a glutaraldehyde solution. Finally, the solution is freeze-dried.	95
10	Gelation	GO is prepared from natural graphite powder by a modified Hummers method and purified by dialysis. To prepare GO hydrogels, a certain volume GO dispersion is mixed with a solution of acid or other cross-linkers. The blend is then shaken to form a hydrogel.	96

9.2.2. Hybrid Composites for Counter Electrodes

Counter electrodes (CEs) in DSSCs have a critical role in determining the cell efficiency depending on their abilities to collect electrons coming from the photoanode side. A number of parameters should be investigated for the selection of optimal and scalable CEs: (1) sheet resistance; (2) catalytic activity; (3) chemical stability; and (4) cost[60,78,98–102]. For an optimized cell, CE sheet resistance must be as low as possible to facilitate electron transport, CE catalytic activity should be very high to effectively reduce redox species, and CE materials must possess a noble-like behavior as in Pt electrodes for corrosion stability[103–106]. Pt is highly expensive for large-scale applications due to its scarcity; the development in Pt-free CEs should be pursued to have cost-effective graphene-based and scalable CEs[78].

Velten et al.[107] utilized spun multi-walled carbon nanotube (MWCNT) sheets with graphene flakes (Gr-F) as CEs achieving a maximum PCE of 7.55% in iodide-based DSSCs; the MWCNTs provided high electrical conductivity whereas Gr-F ensured low charge transfer resistance (R_{ct}), Figure 4(A-C). Choi et al[108] grew graphene MWCNTs on SiO_2/Si which then transplanted onto FTO for utilization as a CE interfaced with TiO_2 and N719 dye yielding in 3% PCE under AM1.5, Figure 4(D,E). Negatively

charged graphene oxide films were also electrochemically reduced (ERGO) *via* a layer-by-layer (LBL) assembly against positively charged PDDA, as shown in Figure 4(F) by Xu et al.[109], for preparing highly efficient graphene-based [PDDA@ERGO] CEs (9.5–7.6%) durable for long-time operation (>1000 h). Chang et al.[110] prepared a novel hybrid 3D graphene nanosheets@ZnO nanorods (GNs@ZnO) nanostructures *via* hydrothermal growth and spin coating methods on FTO for use as CEs, Figure 4(G-I). ZnO nanorods prevent GNs aggregation and allow electrolyte penetration into CEs exposing large surface area of GNs active defective sites for triiodide reduction. The 3D networks significantly improved the CE electrocatalytic activity (due to lower peak separation (E_{pp}) of A_{OX}/A_{RE} redox pair, and higher reduction peak current density (J_{RE}), Figure 4(J), which enhanced electrolyte reduction for high J_{sc} and low charge transfer resistance (R_{ct}), resulting in PCE of 8.12% comparable to Pt-based CE of 8.82%, Figure 4(K)[110]. Another work initiated by Casaluci et al.[111] who spray coated chemically-exfoliated graphene ink on FTO as an alternative to Pt CEs for large-area DSSCs modules (43.2 cm^2) achieving a PCE of 3.5%, Figure 4(M,L). Wang et al.[112] integrated polyaniline (PANI) nanoparticles into graphene sheets *via* in situ polymerization forming graphene/polyaniline nanocomposite as a potential CE for DSSCs with 6.09% PCE achieved from enhancement of CE electrocatalytic performance, Figure 4(N). Dodoo-Arhin et al.[113] fabricated graphene-based CE using stable inkjet printable graphene ink chemically exfoliated from graphite for natural and ruthenium-based DSSCs; dye extracts of C. pulcherrima carotenoids interfaced with inkjet-graphene CE exhibited PCE of 0.9% (attributed to better intermolecular dye interactions) whereas N719 dye showed a relatively high PCE of 3.0% (4.4% when using Pt CEs), Figure 4(O). Yue et al.[114] prepared Pt/graphene hybrid films as CEs for DSSCs using Pt nanoparticles and electrochemical deposition techniques, where

cyclic voltammetry and other electrochemical measurements confirmed the hybrid films had higher conductivity and better electrocatalytic activity towards triiodide reduction than that of pristine Pt electrodes, achieving a high PCE of 7.88%, Figure 4(P).

Kaniyoor and Ramaprabhu [115] identified a low transfer resistance of 11.7 Ω cm^2 that is close enough to Pt (6.5 Ω cm^2) when using thermally exfoliated graphene (TEG) films; system efficiency of 2.8% for TEG was also comparable to that of Pt-based DSSCs (3.4%). Further, Kavan et al.[116] demonstrated that defected graphene structures containing oxygen or –NHCO– groups increase active sites and enhance the electrocatalytic activity of graphene CEs. Under 1-sun illumination, DSSCs modified with carbon-based CEs showed high PCEs of 6.67, 3.9, 4.5, and 7.7% for CEs from graphite[117], activated carbon[118], single-walled carbon nanotubes (SWCNTs)[119] and multi-walled carbon nanotubes (MWCNTs)[120], respectively[78].

The combination of graphene sheets with other carbon materials, Pt, transition metal sulfides, and nitrides provide fast electron diffusion and transport at the electrode-electrolyte interface for system efficiencies up to 7.66, 7.5, and 5.7% for graphene/Pt, graphene/MWCNTs, and $Ni_{12}P_5$/graphene, respectively[78]. Highersr et al.[121] used graphene-NiS_2 as a CE to achieve a PCE of about 8.55%. Nitrogen-doped graphene and/or metal free CEs have been extensively investigated in recent works[122–126], where Xue et al. (2015)[126] fabricated a highly efficient nitrogen-doped graphene nanoribbons (N-GNRs) with a surface area of 751 cm^2 g^{-1} for disulfide/thiolate redox-mediated DSSCs. Incorporation of single metal active sites (Mn, Fe, Co, Ni, and Cu) to the nitrogen atoms doped in graphene leads to composite CEs (e.g. CoN_4/GN) with superior activity, stability, and appropriate adsorption energy as those excellent properties observed in highly stable/expensive metal electrodes (Pt, Au, and Ag)[127].

3D-GBM composites[55,128] are also promising for building DSSCs with enhanced CEs properties. Wang et al.[100] synthesized a 3D honeycomb-like structured graphene (HSG) on a conductive FTO glass to use HSG/FTO as a CE. HSG enhanced the catalytic performance of the cell which resulted in achieving a high efficiency of 7.8% that is comparable to Pt/FTO CEs[55,100]. Tang et al.[128] integrated 3D-GBMs with reduced graphene oxide (rGO) to fabricate a 3D/2D graphene-based CE showing excellent photovoltaic performance as high as 9.79% in DSSCs. The 3D-GBMs network channels are believed to provide fast electron transport while the rGO diminish contact resistance at the graphene/electrolyte interface[128,129]. Sahito et al.[99,130] incorporated cotton fabrics in rGO structure demonstrating a low cost, lightweight, Pt- and metal-free, flexible, cotton-based graphene textile CE for DSSCs. Preparation steps were simple and quick using common dip/dry techniques for adsorption of rGO on cotton fabrics. The novel fiber-based graphene electrode showed excellent bending flexibility, high electrical conductivity, and decent electrocatalytic activity towards reduction of triiodide with a conversion efficiency of 2.52%. Lickleder et al.[131] synthesized a TiS_2 nanotube layer as CEs from the treatment of high temperature H_2S anodized TiO_2 nanotubes; the designed CE showed a very high electrocatalytic activity for the I^-/I_3^- oxidation with DSSCs PCE of 6.1% that is very close to systems with Pt CEs (6.2%)[131].

Table 3. Performance comparison of Various DSSCs: Efficiency and photovoltaic parameter values observed in previously designed DSSCs with different graphene-based counter electrodes.*

Cell Configuration	V_{oc} (V)	J_{sc} (mA/cm^2)	FF (%)	η (%)	Ref.
FTO/TiO_2/N719/Graphene/[I^-/I_3^-]/FTO	0.74	16.99	0.54	6.81	[132]
FTO/TiO_2/N719/Graphene/[I^-/I_3^-]-(AN-50)/FTO	0.54	14.30	0.65	5.69	[133]
ITO/TiO_2/N719/[I^-/I_3^-]/[Graphene/PEDOT-PSS]/ITO	0.72	12.96	0.48	4.50	[134]
FTO/TiO_2/N719/[I^-/I_3^-]/[Graphene/PANI]/FTO	0.68	13.28	0.67	6.09	[112]
FTO/TiO_2/N719/[I^-/I_3^-]/[Graphene/PEDOT]/FTO	0.77	12.60	0.63	6.26	[135]
FTO/TiO_2/N719/[I^-/I_3^-]/[Graphene/Pt]/FTO	0.71	15.20	0.71	7.66	[136]
FTO/TiO_2/N719/[I^-/I_3^-]/ [Graphene/Pt]/FTO	0.79	12.06	0.67	6.35	[137]
FTO/TiO_2/N719/[Graphene/$Ni_{12}P_5$]/[I^-/I_3^-]/FTO	0.74	12.86	0.61	5.70	[138]
FTO/TiO_2/N719/[Graphene/$Ni_{12}P_5$]/[I^-/I_3^-]/FTO	0.70	12.88	0.52	4.70	[138]
ITO/TiO_2/N719/[Graphene/MWCNTs] [I^-/I_3^-]/ITO	0.72	8.95	0.70	4.46	[134]
FTO/TiO_2/N719/ [Graphene/MWCNTs] [I^-/I_3^-]/FTO	0.75	16.05	0.63	7.55	[107]
FTO/TiO_2/N719/[I^-/I_3^-]/[Graphene-(HSG-12 h)]/FTO	0.77	27.20	0.37	7.80	[139]
ITO/TiO_2/N719/[I^-/I_3^-]-(Z946)/[PDDA@ERGO]/ITO	0.69	18.77	0.74	9.54	[109]
ITO/TiO_2/N719/[I^-/I_3^-]-(Z952)/[PDDA@ERGO]/ITO	0.65	15.19	0.76	7.66	[109]
ITO/TiO_2/N719/[I^-/I_3^-]-(Z946)/[PDDA@ERGO]/Pt/ITO	0.69	18.11	0.74	9.14	[109]
FTO/TiO_2/N719/[GNs@ZnO]/[I^-/I_3^-]-(BMII)/FTO	0.76	21.70	0.67	8.12	[110]
FTO/TiO_2/N3/NDG/[I^-/I_3^-]/FTO	0.69	15.76	0.64	7.01	[140]
FTO/TiO_2/N719/Graphene-(0.15wt.%)/[I^-/I_3^-]/FTO	0.75	15.46	0.68	7.88	[114]

*PANI: Polyaniline; PEDOT: Poly(3,4-ethylenedioxythiophene); MWCNTs: Multi-walled carbon nanotubes; HSG: honeycomb-structured graphene; PDDA: Poly(diallyldimethylammonium chloride); ERGO: Electrochemically reduced graphene oxide; GNs: Graphene nanoparticles; NDG: Nitrogen doped graphene

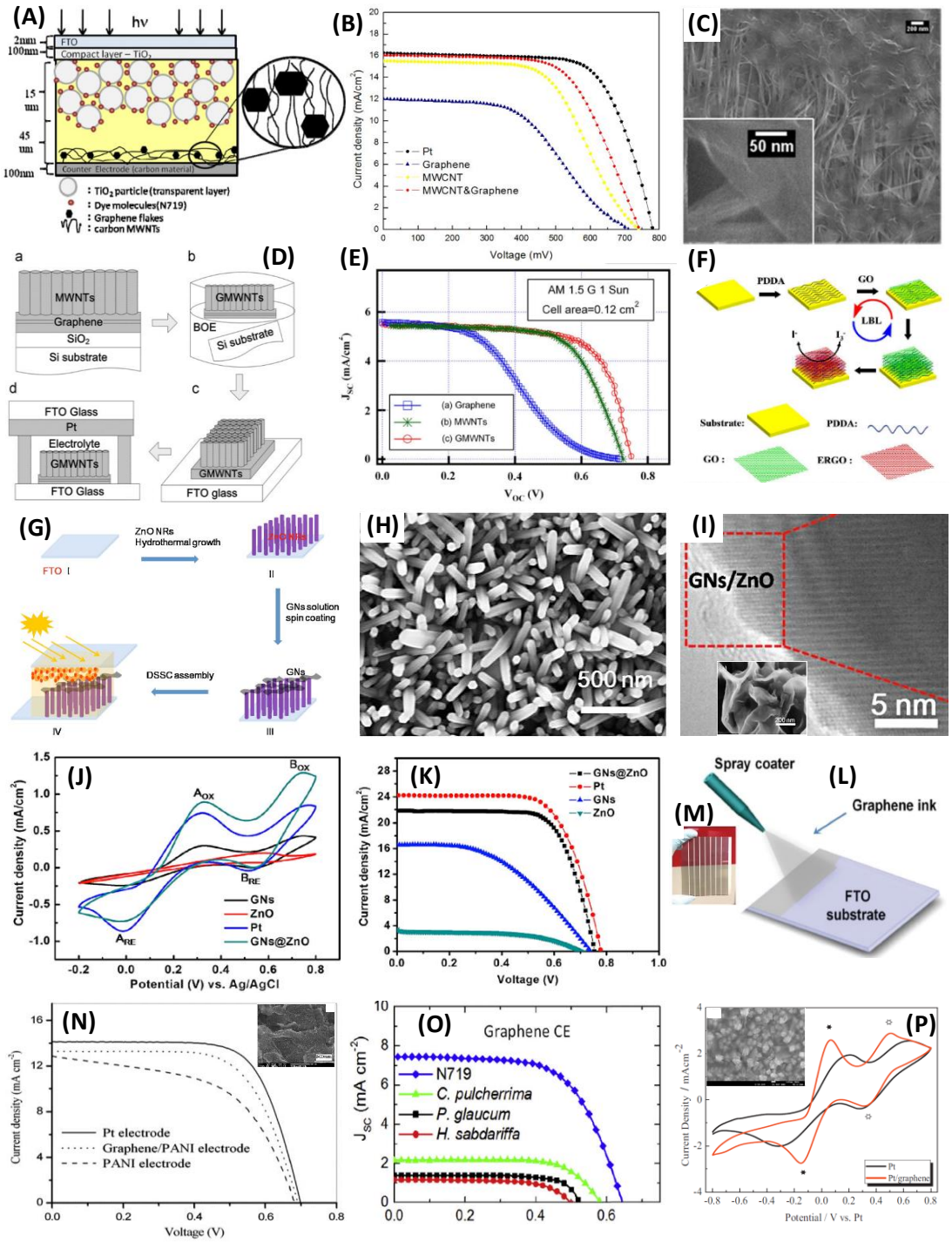

Figure 4. **(A)** Schematic of CNTs/graphene-based DSSCs; **(B)** J–V curves of DSSCs using Pt, graphene, or MWCNTs; **(C)** SEM image of CNTs/graphene composite with inset showing carbon bridges, from[107]; **(D)** Device processing flowchart: (a) GMWNT synthesis, (b) GMWNT lift-off, (c) GMWNT transfer, (d) Pt interface; **(E)** J–V characteristics of DSSCs with different CEs, from[108]; **(F)** Fabrication procedure of [PDDA@ERGO] films, from[109]; **(G)** Preliminary structure and fabrication of ZnO-GNs CE for DSSCs; **(H)** Top-view SEM image of ZnO nanorods on FTO; **(I)** HRTEM image of GNs@ZnO nanorods with inset showing crumpled GNs sheets; **(J)** Cyclic voltammograms (CVs) for GNs, ZnO, GNs@ZnO, and Pt CEs at a scan rate of 50 mV/s; **(K)** J–V curves of DSSCs using different CEs, from[110]; **(L)** Spray coating graphene ink; **(M)** Optical image of graphene-based CE, from[111]; **(N)** J–V curves for graphene/PANI CE based cells with CE SEM image in the inset, from[112]; **(O)** J–V curves for graphene-ink CE based cells, from[113]; **(P)** CVs for Pt and Pt/GN CEs at a scan rate of 10 mV/s with Pt/GN SEM image in the inset, from[114].

9.2.3. Integrated Photoanode-Semiconductor Layers

Graphene quantum dots (GQDs) were applied on TiO_2 films in the photoanode with an optimal controlled amount of $1.7x10^{-4}$ mol/cm^2 by soaking in the GQDs solution at 60 °C for 24 h. The GQDs-modified-photoanode DSSCs showed a maximum J_{sc} of 14.07 mA cm^{-2} and PCE of 6.1% which were approximately 31% and 20%, respectively, higher than current density and efficiency observed in DSSCs devices without GQDs (Figure 5(A,B)). This is attributed to the enhanced photoexcitation response from GQDs along with the dye molecules allowing more electron injection into TiO_2. It is worth mentioning that GTP-1, GTP-2, GTP-3, and GTP-4, from Figure 5(B), refer to 0.025 g, 0.05 g, 0.075 g, and 0.1 g of added GQDs into TiO_2 photoelectrode[141]. Fang et al.[142] used a ball-milling method to prepare G-P25(TiO_2) photoanode electrodes involving addition of different volumes of GO to P-25, which increased the rutile contents with high GO amounts reaching a maximum rutile phase at GO=4.5 mL. A very high interface recombination resistance was observed in the fabricated DSSCs when using G-P25, resulting in PCE of 5.09%, due to the increase in both rutile contents and the porosity achieved by graphene addition (Figure 5(C-E))[142]. Wang et al.[54] utilized graphene-doped TiO_2 films (graphene/TiO_2 composites) in DSSCs which showed a vast improvement in current density by 52%, yielded in enhancing PCE by 55% (from 1.79% to 2.78% dependent on the content of GO). An optimal GO content was obtained at around 0.8 wt. % which believed to maximize photogenerated cell current density due to perfect ratio between dye molecules and graphene content for efficient visible-light harvesting, electron injection, forward transport, and extended electron lifetime (Figure 5(F-I))[54].

Sun et al.[77] prepared graphene-TiO_2 nanocomposite photoanodes by heterogeneous coagulation between TiO_2 P25 nanoparticles and Nafion-coated graphene for strong

interfacial binding and attachment of deposited graphene. The high graphene theoretical specific surface area (2630 m^2/g) ensures ideal interfacial contact and strong electrostatic attraction between graphene and TiO_2 even at small amounts of added graphene. The incorporation of only 0.5 wt. % of graphene (i.e. graphene-to-P25 ratio = 1:200) demonstrated a significant PCE of 4.28% and 8.38 mA/cm^2, which enhanced efficiency by 59% and current density by 66% as compared to cells without graphene (Figure 5(J-L)[77]. Deposited graphene platelets yielded in increasing dye molecules adsorption and significantly increased electron lifetime from the provided rapid electron pathways. Lim et al. integrated reduced graphene oxide (rGO) into TiO_2 to create (rGO–TiO_2) nanocomposite photoanodes which achieved high DSSCs efficiency of 5.83%. It was found that 0.5 mg would be the optimal rGO content for TiO_2 in order to have high photons absorption as well as reduced back electron transport boosting charge collection (Figure 5(M,N))[143]. When a compact layer of TiO_2 was deposited *via* AACVD between the ITO and the rGO–TiO_2, the DSSCs generated an increased current density of 550% reaching J_{sc}=13.43 mA/cm^2 that was responsible for the highly observed PCE. Introduced compact layer in the photoanode further enhanced forward electron transfer from dye and/or electrolyte to TiO_2 and ITO owing to the extra charge transfer pathways provided by embedded rGO[143].

Table 4. Performance comparison of Various DSSCs: Efficiency and photovoltaic parameter values observed in previously designed DSSCs with different graphene-based photoanodes.

Cell Configuration	V_{oc} (V)	J_{sc} (mA/cm^2)	FF (%)	η (%)	Ref.
FTO/TiO_2/anthocyanin/[I^-/I_3^-]-(BMII)/Pt/FTO	N/A	1.63	0.51	0.51	144
FTO/GO/TiO_2/[purple-cabbage-dye]/[I^-/I_3^-]-(LiI+I_2+PMII)/Pt/FTO	0.31	0.22	0.31	0.36	145
FTO/TiO_2/GQDs/N719/[I^-/I_3^-]-(LiI+I_2+PMII)/Pt/FTO	0.66	14.07	0.59	6.10	141
FTO/TiO_2/GO/[I^-/I_3^-]-(LiI+I_2+PMII)/Pt/FTO	0.61	10.28	0.63	5.09	142
FTO/TiO_2/GO/N719/[I^-/I_3^-]-(LiI+I_2+TBP+MPN)/Pt/FTO	0.67	7.60	0.54	2.78	54
FTO/Graphene/TiO_2/N719/Electrolyte/Pt/FTO	0.73	8.38	N/A	4.28	77
ITO/rGO-TiO_2/N719/Iodolyte-(Z-100)/Pt/ITO	0.74	13.43	0.59	5.83	143
ITO/TiO_2/Graphene/N719/[I^-/I_3^-]/Pt/ITO	0.70	19.92	0.48	6.86	146
FTO/TiO_2/Graphene/N719/[I^-/I_3^-]-(LiI+I_2+PMII)/Pt/FTO	0.67	16.80	0.56	5.77	147
FTO/TiO_2/Graphene/N719/[I^-/I_3^-]/Pt/FTO	0.68	12.89	0.69	6.05	148

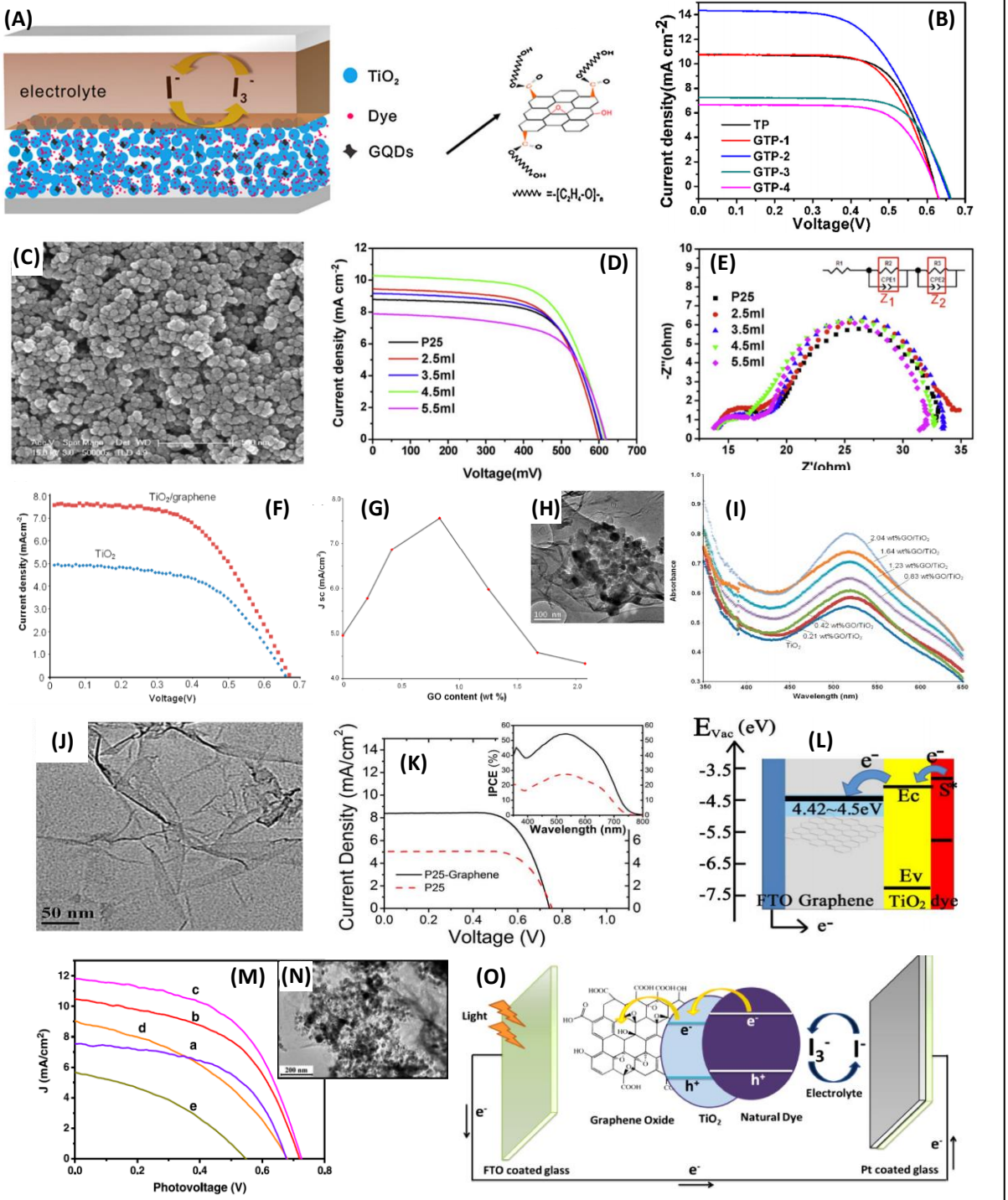

Figure 5. (A) Configuration of GQDs modified DSSCs with PEG-passivated GQDs structure; **(B)** J–V curves of DSSCs using different GQDs weights (cell area of 0.25 cm^2), from[141]; **(C)** SEM image of G-P25 photoelectrode with GO=4.5 mL; **(D)** J–V curves; and **(E)** Nyquist plots of DSSCs with different GO contents for G-P25, from[142]; **(F)** Performance of TiO_2/GO-based DSSCs; **(G)** J_{sc} vs. GO content; **(H)** Morphology of 0.83 wt. % GO/TiO_2 composite; **(I)** UV/Vis absorbance spectra, from[54]; **(J)** TEM image of the graphene dispersed by Nafion; **(K)** J–V characteristics of DSSCs with P25 and P25-graphene; **(L)** Energy band matching diagram, from[77]; **(M)** J–V curves obtained for rGO–TiO_2 nanocomposite-modified photoanodes with (a) 0.05, (b) 0.1, (c) 0.5, (d) 1, and (e) 2 mg of rGO content; **(N)** HRTEM image of rGO–TiO_2, from[143]; **(O)** Electron transport/generation using GO/TiO_2 modified-photoanode for DSSCs; from[145].

9.3 Biomolecular Dyes for Naturally-Sensitized Photoanodes

The integration of natural dyes in DSSCs holds a potential towards fabricating low cost environmental-friendly cells operating with toxic-free sensitizers[56,59,61,149]. Different biomolecular sources as fruits, flowers, leaves and bacteria complexes can be used to extract anthocyanin, carotenoid, flavonoid, aurone, and chlorophyll etc.[150,151]. Highly conjugated double bonds structure is desired when selecting natural sensitizers to ensure visible-light absorption in the range 400–700 nm[50,152]. Carotenoids are promising candidates for strong light absorption at 400–500 nm owing to their long chain length of more than seven conjugated π bonds[153]. However, the highest observed efficiency in DSSCs using plant-based carotenoid pigments is <2.6%[154] that can be further enhanced to 4.2%[155] from chlorophyll integration as in tested systems with chlorophyll/β-carotene, chlorophyll/lutein, chlorophyll/violaxanthin, and chlorophyll/neoxanthin[155]. The enhancement of visible-light absorption and expansion of the photoanode absorbance range can be achieved by the addition of 3D-GBMs as either a sensitizer or anode-modified electrode integrated with photoactive layers[156].

According to Hug et al. (2014)[59], many other natural sensitizers such as bixin, crocetin, crocin, betaxanthin, betalains, mangostin, rutin, neoxanthin, violaxanthin, and lutein have been previously extracted from plant sources and tested in DSSCs showing fairly good photons-to-electrons conversions. For instance, rutin extracts from either mangosteen pericarp or Rhoeo spathacea recorded a high naturally-sensitized DSSCs performance in the range 1.17–1.49%[157]. A higher conversion efficiency of 2.06%[158] was achieved from using betaxanthin pigments extracted from Sicilian prickly pear. Interestingly, anthocyanin from black rice and rosa xanthine showed PCE of 1.63–3.27%[159], capsicum carotenoid showed 0.58%[159], cyanine dyes 4.8–7.62%[160,161], coumarin pigments 7.7–9% [162,163] under 1 sun radiation (100 mW/cm^2).

The use of cobalt solid-state redox with novel metal-free organic dye (DHO-TPA)-Dye 1 in DSSCs increases dye attachment and cell stability with performance that can reaches up to 10.3%[164]. The alternative selection of natural and/or bacterial sensitizers arise because of the many advantages achieved when using biomolecular sensitizers over commercial metal-based dyes[165,166]. Application and integration of such toxic-free dyes in the photoanode structure modified with graphene-based materials sounds promising due to the following reasons: (i) plant-based and bacteria-based natural sensitizers are abundant and cost-effective, (ii) dye extraction is not difficult and can be easily done *via* solvent, aqueous, or acid extraction, (iii) natural pigments are toxic-free and environmental-friendly with unknown health risks to humans, (iv) metal-free dyes are sustainable, biodegradable, and can be reextracted or quantity-wise scaled according to the system needs, and (v) the mixing of both graphene with dye sensitizers assure photoanode's wide absorbance ranges in the visible-light spectrum for enhance photocurrents[50,61,165,166].

DSSCs sensitized by chlorophyll, carotenoids, or other proteins pigment complexes, extracted from plant or bacteria sources, usually show low performance which can be further improved from addition of graphene-based materials in the photoanode. To the authors' knowledge, there are no much studies focus on integration of graphene and/or 3D-GBMs with natural sensitizers as an attempt to increase photoanode visible-light sensitivity, which would enhance both electron injection and forward transport for more generated photocurrents. Graphene have been previously added to dye and titania in red cabbage anthocyanin-based DSSCs which achieved a 2.4-fold increase in PCE using graphene-to-titania dispersion with 3:5 volumetric ratio. The increased efficiency is attributed to the enhanced short-circuit current (J_{sc}) since co-adsorbed graphene onto anthocyanin molecules and/or titania photoanode provide conductive

electron pathways. These pathways ensure only forward electron transport developing photo-generated currents[144]. Al-Ghamdi et al. (2014) introduced pre-synthesized graphene oxide (GO), using the modified Hummer's method, into a purple cabbage naturally-sensitized TiO_2 photoanode for DSSCs as shown in Figure 5(O). The introduction of GO improved the overall cell performance from 0.15% to 0.36%, which is believed to increase due to the enhanced visible-light absorption capabilities from graphene and provided electron pathways for forward charge transport[145].

Recent studies showed the potential in using biomolecular sensitizers in photoanode structures. In 2019, a theoretical work based on density functional theory (DFT) initiated by Zanjanchi and Beheshtian concluded that carotenoids, chlorophylls, and anthocyanins are the optimal natural pigment classes to have high open-circuit photovoltage[167]. Experimental works backed-up this theory where Pandey (2018) found that a highest PCE of 2% is possible to achieve in DSSCs *via* improving photoanode visible-light absorption abilities using cocktail of naturally-sensitized dyes (e.g. chlorophyll, betanins, carotenoids, anthocyanins, and tannins)[168]. Another study established a comparison between various plant-based biomolecular pigments such as chlorophyll, carotenoid, betalains and anthocyanin when used in a TiO_2-based DSSCs. The maximum PCE of 1.3–6.7%[169,170] was observed for chlorophyll (from chlorin e6 derivative 6) extracted from Shiso leaves and deposited onto a TiO_2 photoanode with p-CuI electrolyte; pomegranate showed PCE of 2%[170,171]; [A. amentacea + P. pterocarpum] plant-based pigments recorded a max PCE of 7.38–8.22%[170,172]. Incorporation of betalains, carotenoids and chlorophylls, extracted from vegetable[173], in bio-sensitized DSSCs resulted in a maximum PCE of 2.06% using betalains (Sicilian pear)[158], 0.37% using carotenoids (Annatto)[174], and 4.6% using chlorophylls (Wakame)[175].

9.3.1. Sources of Bio-Sensitizers

The extraction of biomolecular photosensitizers occurs by isolation of passive or active bacterial cells and complex molecules exist in the cytoplasm. Protein pigment complexes created by the bacteria cytoplasm (e.g. Ribosomes) generates LH2, LH4, and RC pigments or hydrogenase enzymes perfect for solar-to-energy applications[176–178]. Similarly, plant-based biological systems (e.g. plants, algae, and fungi) produce orange-reddish carotenoids pigments by photosynthesis for protection against excess UV/oxidation damage[179–181]. Chlorophyll pigments are photosynthetically synthesized in various plants and cyanobacteria which can be used to harvest visible-light energy in sensitized solar cells[59,150,182]. Table 5 shows the common discussed natural pigments and their possible bacterial sources.

Table 5. Bacterial sources of various discussed natural pigments for bio-sensitized DSSCs

Bio-pigment	Bacterial Source	Ref.
RC Proteins	Rb. sphaeroides (purple non-sulfur bacteria); bacterium RS601;[183] M. pneumoniae; M. genitalium; B. subtilis; S. sanguinis; H. pylori; C. crescentus; P. aeruginosa and E. coli[184]	183,184
Chlorophyll a (BChl)	Purple bacteria, Heliobacteria, Green sulfur bacteria, Chloroflexi	185
Carotenoids	Rhodobacter sphaeroides G1C, Rhodobacter sphaeroides 2.4.1, Allochromatium vinosum and Rhodospirillum rubrum S1	182
LH2, LH4 and RC proteins pigment complexes (PPCs)	Purple bacteria, specifically, Rhodopseudomonas palustris CQV97 and Rhodobacter azotoformans R7	186

9.3.2. Donor-π-Acceptor Photosensitizer Structure

The chemical structure of a photosensitizer involves a donor-acceptor-substituted π-conjugated bridge[187], where donor and acceptor moieties within the dyes control how efficiently dye molecules take electrolyte electrons (donor) to be excited and injected

to the semiconductor *via* acceptor segments[188]. The pigment molecular structure, anchoring functional groups, hydrocarbon chain length, and number of conjugated double bonds (n) in biomolecular pigments are very important to study for the selection of ideal bio-pigments for DSSCs (Figure 6). Using dyes with wider absorbance ensures intense visible-light absorption. Pigment complexes with lots of hydroxyl (–OH) and carboxyl (–COOH) radicals provide strong binding and chemisorption of dye molecules onto the semiconductor; thereby, lowering electron resistance and facilitating electron injection[182,189]. Integrating phenyl units in these moieties can effectively improve electron transport and reduce recombination for high PCE[190]. Moreover, bulky alkyl chains or aromatics incorporated in pigment's spacer segments inhibit dye aggregation for increased charge lifetime[188].

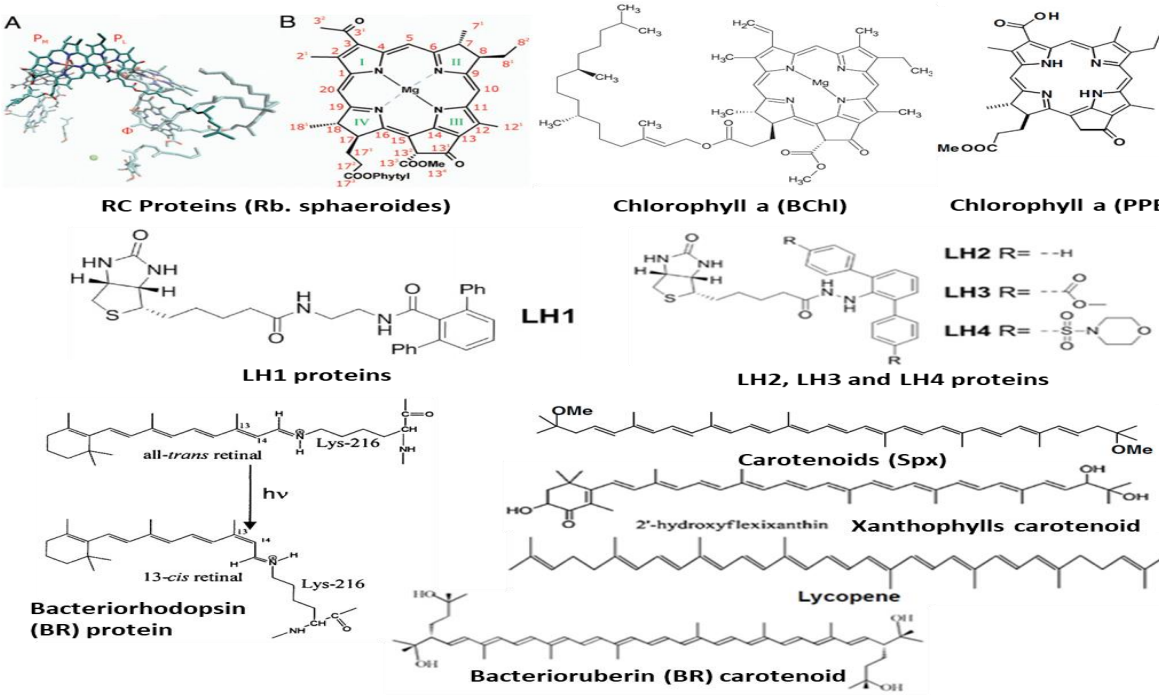

Figure 6. Chemical structure of different biomolecular pigments, from[67].

9.3.3. Bandgap for Photoexcitation of π-Conjugated Electrons

Pigment gap energies can be calculated from the difference between HOMO to LUMO levels, associated with the molecular orbital and electron distribution[191,192], ($E_g = E_{LUMO} - E_{HOMO}$), which should be typically lower than the semiconductor bandgap. For instance, cyanine dyes HOMO (–5.73 eV), LUMO (–3.82 eV) which would result in a molecular cyanine gap energy of 1.91 eV[161]. When dye LUMO level is higher than that of the semiconductor, excited electrons get injected into the conduction band of the semiconductor. Dye absorption abilities depend exclusively on HOMO and LUMO potential levels. The difference between HOMO in the dye and the redox potential of the electrolyte needs to be high for driving electron diffusion[158].

Table 6. HOMO/LUMO energy levels of different and common biomolecular dyes

Pigment Category and/or TiO_2	Theoretical/ Experimental	HOMO-to-LUMO Energy (eV)*	Ref.
Anthocyanin	Theoretical	2 – 2.78	193
	Experimental	2.18 – 3.26	193
Carotenoid	Theoretical	2.2 – 7.3	194,195
	Experimental	N/A	194
Chlorophyll	Theoretical	4.14	196
	Experimental	1.82	196
Cyanine	Theoretical	1 – 1.5	197,198
	Experimental	1.5 – 2.2	197
Xanthene	Theoretical	1.74 – 3.95	199–201
	Experimental	N/A	199
Coumarin	Theoretical	1.25 – 2.93	202,203
	Experimental	2.08 – 3.49	202
TiO_2	Theoretical	4.18	203
	Experimental	3.49	203

*HOMO/LUMO energies determined from theoretical time-dependent and density functional theory (TD-DFT)

It is more probable that low dye bandgaps result in easy electron excitation and excitons generation in the HOMO levels. Anthocyanin, cyanine, and coumarin dyes had the highest bio-sensitized DSSCs PCEs >3.27% and up to 9% due to their low

HOMO/LUMO energies <2.46 eV. Table 6 shows the theoretical HOMO/LUMO energy levels for biomolecular dyes and their corresponding gap energy (in eV) required for electron photoexcitation.

9.3.4. Carotenoids and Other Biomolecular Pigments

Carotenoids show strong pigment colors due to the presence of conjugated π-electrons in their conjugated structure. Pigments from carotenoids only show up when the number of conjugated double bonds is (n>8), where systems with few conjugations (n<8) can only absorb UV-light and high photons energy. Highly conjugated systems absorb low and/or visible-light energy whereas molecular structures with fewer conjugated bonds absorb high energies[204–206]. The blending of chlorophyll with carotenoids has shown much improvements in carotenoids sensitizing function in DSSCs since chlorophyll provides intensified visible-light absorption capabilities with enhanced layer protection[207,208] and formed radical cations[209]. Protein complexes (LH2, BR, RC) and chlorophyll a combined with carotenoids showed a high DSSCs PCE of 0.16–0.57% and 4%, respectively. On the contrary, xanthophylls carotenoids showed a low PCE of 0.008–0.03% as compared with other biomolecular pigments. The use of co-adsorbents boosted up PCE to 0.03% due to strong dye attachment enhancing charge transport and electron injection (Table 7).

568 **Table 7.** PCE comparison between various bio-sensitized DSSCs when using
569 different/common biomolecular pigments under AM1.5 radiation.*

Bacterial Pigment	J_{sc} (μA cm^{-2})	V_{oc} (mV)	FF	$\eta*$ (%)	Ref.
Chlorophyll a (PPB) + Carotenoids (Spx)	11500	-	-	4	182
Chromatophores	24.7	300	0.29	0.04	45
PPCs (LH2)	1460	620	0.54	0.49	186
PPCs (RC)	1240	840	0.55	0.57	186
Light-harvesting complex II (LHCII)	800	590	0.58	0.27	210
Bacteriorhodopsin proteins and bacterioruberin carotenoids (BRs)	450	570	0.62	0.16	61
Xanthophylls carotenoids (yellow)	130	549	-	0.0323	50
Xanthophylls carotenoids (red)	200	435	-	0.0332	50
Xanthophylls carotenoids (PURE orange)	78	260	0.39	0.008	211
Xanthophylls carotenoids (RAW orange)	127	460	0.51	0.03	211
Xanthophylls carotenoids (Cocktail)	98	260	0.38	0.009	211
Lycopene carotenoids	696	289	-	0.057	212
RC photosystem I trimer (PSI)	362	500	0.71	0.08	213
Bacteriorhodopsin (BR) protein	620	-	-	0.19	214
Bacteriorhodopsin (BR) protein	1008	-	-	0.49	214

570 * J_{sc} = Short-circuit current density; V_{oc} = Open-circuit voltage; FF = Fill factor; η = Incident photon-to-
571 current efficiency (IPCE) = Quantum efficiency (QE).
572

573 ## 9.4 Conclusion

574 In conclusion, this chapter highlights the promising role of 3D-GBMs as electrodes for
575 the enhancement of photocurrent generation and charge carriers transport in DSSCs.
576 Interconnected networks and channels in 3D-GBMs provide extra electron pathways
577 and large specific surface area for improved electron transport and enhanced dye
578 adsorption in the photoanode, respectively. Large scale processing of 3D-GBMs
579 based composite electrodes is advantageous for producing cost-effective and large
580 DSSCs modules. Additionally, employing environmental-friendly sensitizers including

biomolecular dyes with 3D-GBMs for hybrid photoanode architectures will further facilitate exciton generation and electron forward transport owing to the highly conjugated dye double bonds structure and interconnected graphene channels. Further studies on charge transport mechanism, carriers' lifetimes, dye-graphene interaction, graphene-semiconductor adhesion, 3D-GBMs composition, and photoanode electronic properties should be tackled for better understanding of advanced DSSCs.

References

1 B. Parida, S. Iniyan and R. Goic, *Renew. Sustain. Energy Rev.*, 2011.

2 X. Pi, L. Zhang and D. Yang, *J. Phys. Chem. C*, , DOI:10.1021/jp307078g.

3 H. F. W. Dekkers, L. Carnel and G. Beaucarne, *Appl. Phys. Lett.*, , DOI:10.1063/1.2219142.

4 M. Lipiński, P. Panek, Z. Witek, E. Beltowska and R. Ciach, in *Solar Energy Materials and Solar Cells*, 2002.

5 E. Klampaftis and B. S. Richards, *Prog. Photovoltaics Res. Appl.*, , DOI:10.1002/pip.1019.

6 D. Sarti and R. Einhaus, *Sol. Energy Mater. Sol. Cells*, , DOI:10.1016/S0927-0248(01)00147-7.

7 N. K. Noel, S. D. Stranks, A. Abate, C. Wehrenfennig, S. Guarnera, A. A. Haghighirad, A. Sadhanala, G. E. Eperon, S. K. Pathak, M. B. Johnston, A. Petrozza, L. M. Herz and H. J. Snaith, *Energy Environ. Sci.*, , DOI:10.1039/c4ee01076k.

8 L. Tzounis, T. Stergiopoulos, A. Zachariadis, C. Gravalidis, A. Laskarakis and S. Logothetidis, in *Materials Today: Proceedings*, 2017.

9 W. Zhang, G. E. Eperon and H. J. Snaith, *Nat. Energy*, 2016.

10 M. Liu, M. B. Johnston and H. J. Snaith, *Nature*, , DOI:10.1038/nature12509.

11 N. G. Park, *Mater. Today*, 2015.

12 M. A. Green, A. Ho-Baillie and H. J. Snaith, *Nat. Photonics*, 2014.

13 H. Zhou, Q. Chen, G. Li, S. Luo, T. B. Song, H. S. Duan, Z. Hong, J. You, Y. Liu and Y. Yang, *Science (80-.).*, , DOI:10.1126/science.1254050.

14 G. Hodes, *Science (80-.).*, 2013.

15 H. S. Jung and N. G. Park, *Small*, 2015.

16 M. Tao, *Electrochem. Soc. Interface*.

17 R. W. Miles, G. Zoppi and I. Forbes, *Mater. Today*, , DOI:10.1016/S1369-7021(07)70275-4.

18 B. E. McCandless and J. R. Sites, in *Handbook of Photovoltaic Science and Engineering*, 2011.

19 J. Britt and C. Ferekides, *Appl. Phys. Lett.*, , DOI:10.1063/1.109629.

20 X. Wu, *Sol. Energy*, , DOI:10.1016/j.solener.2004.06.006.

21 M. Kaelin, D. Rudmann and A. N. Tiwari, *Sol. Energy*, , DOI:10.1016/j.solener.2004.08.015.

22 R. Wuerz, A. Eicke, M. Frankenfeld, F. Kessler, M. Powalla, P. Rogin and O. Yazdani-Assl, *Thin Solid Films*, , DOI:10.1016/j.tsf.2008.11.016.

23 T. Wada, Y. Hashimoto, S. Nishiwaki, T. Satoh, S. Hayashi, T. Negami and H. Miyake, *Sol. Energy Mater. Sol. Cells*, , DOI:10.1016/S0927-0248(00)00296-8.

24 E. Cuce, C.-H. Young and S. B. Riffat, *Energy Build.*, , DOI:10.1016/j.enbuild.2014.10.063.

25 T. Ameri, G. Dennler, C. Lungenschmied and C. J. Brabec, *Energy Environ. Sci.*, 2009.

26 S. Albrecht, S. Yilmaz, I. Dumsch, S. Allard, U. Scherf, S. Beaupré, M. Leclerc and D. Neher, in *Energy Procedia*, 2011.

27 A. Hadipour, B. De Boer and P. W. M. Blom, *Adv. Funct. Mater.*, , DOI:10.1002/adfm.200700517.

28 T. Ameri, N. Li and C. J. Brabec, *Energy Environ. Sci.*, 2013.

29 M. Riede, C. Uhrich, J. Widmer, R. Timmreck, D. Wynands, G. Schwartz, W. M. Gnehr, D. Hildebrandt, A. Weiss, J. Hwang, S. Sundarraj, P. Erk, M. Pfeiffer and K. Leo, *Adv. Funct. Mater.*, , DOI:10.1002/adfm.201002760.

30 L. Meng, Y. Zhang, X. Wan, C. Li, X. Zhang, Y. Wang, X. Ke, Z. Xiao, L. Ding, R. Xia, H. L. Yip, Y. Cao and Y. Chen, *Science (80-.).*, , DOI:10.1126/science.aat2612.

31 K. Tvrdy and P. V. Kamat, in *Comprehensive Nanoscience and Technology*, 2010.

32 R. A. Taylor and K. Ramasamy, *SPR Nanosci.*, , DOI:10.1039/9781782620358-00142.

33 Z. Pan, H. Rao, I. Mora-Seró, J. Bisquert and X. Zhong, *Chem. Soc. Rev.*,

2018.

34 P. V. Kamat, *J. Phys. Chem. C*, , DOI:10.1021/jp806791s.

35 A. J. Nozik, M. C. Beard, J. M. Luther, M. Law, R. J. Ellingson and J. C. Johnson, *Chem. Rev.*, , DOI:10.1021/cr900289f.

36 Z. Ning, X. Gong, R. Comin, G. Walters, F. Fan, O. Voznyy, E. Yassitepe, A. Buin, S. Hoogland and E. H. Sargent, *Nature*, , DOI:10.1038/nature14563.

37 B. O'Regan and M. Grätzel, *Nature*, , DOI:10.1038/353737a0.

38 Y. Koyama, T. Miki, X. F. Wang and H. Nagae, *Int. J. Mol. Sci.*, 2009.

39 L. Kavan, *Curr. Opin. Electrochem.*, 2017.

40 A. Hagfeldt, in *Ambio*, 2012.

41 T. Bessho, S. M. Zakeeruddin, C. Y. Yeh, E. W. G. Diau and M. Gr??tzel, *Angew. Chemie - Int. Ed.*, , DOI:10.1002/anie.201002118.

42 K. V. Hemalatha, S. N. Karthick, C. Justin Raj, N. Y. Hong, S. K. Kim and H. J. Kim, *Spectrochim. Acta - Part A Mol. Biomol. Spectrosc.*, , DOI:10.1016/j.saa.2012.05.027.

43 S. Ito, H. Miura, S. Uchida, M. Takata, K. Sumioka, P. Liska, P. Comte, P. Péchy and M. Grätzel, *Chem. Commun.*, , DOI:10.1039/b809093a.

44 B. Tan, E. Toman, Y. Li and Y. Wu, *J. Am. Chem. Soc.*, , DOI:10.1021/ja070804f.

45 K. Woronowicz, S. Ahmed, A. A. Biradar, A. V. Biradar, D. P. Birnie, T. Asefa and R. A. Niederman, *Photochem. Photobiol.*, , DOI:10.1111/j.1751-1097.2012.01190.x.

669 46 S. M. Feldt, E. A. Gibson, E. Gabrielsson, L. Sun, G. Boschloo and A.
670 Hagfeldt, *J. Am. Chem. Soc.*, , DOI:10.1021/ja1088869.

671 47 C. Dette, M. a. Pérez-Osorio, C. S. Kley, P. Punke, C. E. Patrick, P. Jacobson,
672 F. Giustino, S. J. Jung and K. Kern, *Nano Lett.*, 2014, **14**, 6533–6538.

673 48 J. D. Roy-Mayhew and I. A. Aksay, *Chem. Rev.*, 2014.

674 49 I. McConnell, G. H. Li and G. W. Brudvig, *Chem. Biol.*, ,
675 DOI:10.1016/j.chembiol.2010.05.005.

676 50 N. Órdenes-Aenishanslins, G. Anziani-Ostuni, M. Vargas-Reyes, J. Alarcón, A.
677 Tello and J. M. Pérez-Donoso, *J. Photochem. Photobiol. B Biol.*, ,
678 DOI:10.1016/j.jphotobiol.2016.08.004.

679 51 C. Y. Chen, M. Wang, J. Y. Li, N. Pootrakulchote, L. Alibabaei, C. H. Ngoc-Le,
680 J. D. Decoppet, J. H. Tsai, C. Grätzel, C. G. Wu, S. M. Zakeeruddin and M.
681 Grätzel, *ACS Nano*, , DOI:10.1021/nn900756s.

682 52 W. Wu, X. Xu, H. Yang, J. Hua, X. Zhang, L. Zhang, Y. Long and H. Tian, *J.*
683 *Mater. Chem.*, , DOI:10.1039/c1jm10942a.

684 53 S. Chowdhury and R. Balasubramanian, *Prog. Mater. Sci.*, 2017.

685 54 H. Wang, S. L. Leonard and Y. H. Hu, *Ind. Eng. Chem. Res.*, ,
686 DOI:10.1021/ie300563h.

687 55 S. Mao, G. Lu and J. Chen, *Nanoscale*, 2015.

688 56 M. R. Narayan, *Renew. Sustain. Energy Rev.*, 2012.

689 57 S. Mathew, A. Yella, P. Gao, R. Humphry-Baker, B. F. E. Curchod, N. Ashari-
690 Astani, I. Tavernelli, U. Rothlisberger, M. K. Nazeeruddin and M. Grätzel, *Nat.*

Chem., , DOI:10.1038/nchem.1861.

58 M. Ye, X. Wen, M. Wang, J. Iocozzia, N. Zhang, C. Lin and Z. Lin, *Mater. Today*, 2015.

59 H. Hug, M. Bader, P. Mair and T. Glatzel, *Appl. Energy*, , DOI:10.1016/j.apenergy.2013.10.055.

60 V. Sugathan, E. John and K. Sudhakar, *Renew. Sustain. Energy Rev.*, 2015.

61 A. Molaeirad, S. Janfaza, A. Karimi-Fard and B. Mahyad, *Biotechnol. Appl. Biochem.*, , DOI:10.1002/bab.1244.

62 M. K. Nazeeruddin, E. Baranoff and M. Grätzel, *Sol. Energy*, , DOI:10.1016/j.solener.2011.01.018.

63 J. Gong, K. Sumathy, Q. Qiao and Z. Zhou, *Renew. Sustain. Energy Rev.*, 2017.

64 L. Kavan, *Chem. Rec.*, , DOI:10.1002/tcr.201100012.

65 J. Gong, J. Liang and K. Sumathy, *Renew. Sustain. Energy Rev.*, 2012.

66 T. Marinado, 2009.

67 H. Maddah, V. Berry and S. Behura, *Renew. Sustain. Energy Rev.*

68 J. B. Asbury, E. Hao, Y. Wang, H. N. Ghosh and T. Lian, *J. Phys. Chem. B*, , DOI:10.1021/jp003485m.

69 A. Hagfeldt and M. Grätzel, *Chem. Rev.*, , DOI:10.1021/cr00033a003.

70 S. Rühle and D. Cahen, *J. Phys. Chem. B*, , DOI:10.1021/jp047686s.

71 P. J. Cameron, L. M. Peter and S. Hore, *J. Phys. Chem. B*, ,

DOI:10.1021/jp0405759.

72 P. J. Cameron and L. M. Peter, *J. Phys. Chem. B*, , DOI:10.1021/jp0407270.

73 H. Yu, S. Zhang, H. Zhao, G. Will and P. Liu, *Electrochim. Acta*, , DOI:10.1016/j.electacta.2008.09.025.

74 N. Koumura, Z. S. Wang, S. Mori, M. Miyashita, E. Suzuki and K. Hara, *J. Am. Chem. Soc.*, , DOI:10.1021/ja0645640.

75 M. Miyashita, K. Sunahara, T. Nishikawa, Y. Uemura, N. Koumura, K. Hara, A. Mori, T. Abe, E. Suzuki and S. Mori, *J. Am. Chem. Soc.*, , DOI:10.1021/ja803534u.

76 E. Palomares, J. N. Clifford, S. A. Haque, T. Lutz and J. R. Durrant, *J. Am. Chem. Soc.*, , DOI:10.1021/ja027945w.

77 S. Sun, L. Gao and Y. Liu, *Appl. Phys. Lett.*, , DOI:10.1063/1.3318466.

78 Y. H. Wang, H., & Hu, *Energy Environ. Sci.*, 2012, **5**, 8182–8188.

79 K. S. Novoselov, A. K. Geim, S. V. Morozov, D. Jiang, Y. Zhang, S. V. Dubonos, I. V. Grigorieva and A. A. Firsov, *Science (80-.).*, , DOI:10.1126/science.1102896.

80 X. Du, I. Skachko, A. Barker and E. Y. Andrei, *Nat. Nanotechnol.*, , DOI:10.1038/nnano.2008.199.

81 A. Peigney, C. Laurent, E. Flahaut, R. R. Bacsa and A. Rousset, *Carbon N. Y.*, , DOI:10.1016/S0008-6223(00)00155-X.

82 R. R. Nair, P. Blake, A. N. Grigorenko, K. S. Novoselov, T. J. Booth, T. Stauber, N. M. R. Peres and A. K. Geim, *Science (80-.).*, ,

DOI:10.1126/science.1156965.

83 Y. Zhang, H. Li, L. Kuo, P. Dong and F. Yan, *Curr. Opin. Colloid Interface Sci.*, 2015.

84 X. Wang, L. Zhi and K. Müllen, *Nano Lett.*, , DOI:10.1021/nl072838r.

85 M. Kotal, J. Kim, J. Oh and I. K. Oh, *Front. Mater.*, 2016.

86 Y. Shen, Q. Fang and B. Chen, *Environ. Sci. Technol.*, 2015.

87 Z. Chen, W. Ren, L. Gao, B. Liu, S. Pei and H. M. Cheng, *Nat. Mater.*, , DOI:10.1038/nmat3001.

88 L. Qiu, J. Z. Liu, S. L. Y. Chang, Y. Wu and D. Li, *Nat. Commun.*, , DOI:10.1038/ncomms2251.

89 R. Menzel, S. Barg, M. Miranda, D. B. Anthony, S. M. Bawaked, M. Mokhtar, S. A. Al-Thabaiti, S. N. Basahel, E. Saiz and M. S. P. Shaffer, *Adv. Funct. Mater.*, , DOI:10.1002/adfm.201401807.

90 C. Zhu, T. Y. J. Han, E. B. Duoss, A. M. Golobic, J. D. Kuntz, C. M. Spadaccini and M. A. Worsley, *Nat. Commun.*, , DOI:10.1038/ncomms7962.

91 X. Xiao, T. E. Beechem, M. T. Brumbach, T. N. Lambert, D. J. Davis, J. R. Michael, C. M. Washburn, J. Wang, S. M. Brozik, D. R. Wheeler, D. B. Burckel and R. Polsky, *ACS Nano*, , DOI:10.1021/nn300655c.

92 Z. Tang, S. Shen, J. Zhuang and X. Wang, *Angew. Chemie - Int. Ed.*, , DOI:10.1002/anie.201000270.

93 H. Hu, Z. Zhao, W. Wan, Y. Gogotsi and J. Qiu, *Adv. Mater.*, , DOI:10.1002/adma.201204530.

94 X. Zhang, Z. Sui, B. Xu, S. Yue, Y. Luo, W. Zhan and B. Liu, *J. Mater. Chem.*, , DOI:10.1039/c1jm10239g.

95 J. Y. Hong, B. M. Bak, J. J. Wie, J. Kong and H. S. Park, *Adv. Funct. Mater.*, , DOI:10.1002/adfm.201403273.

96 H. Bai, C. Li, X. Wang and G. Shi, *J. Phys. Chem. C*, , DOI:10.1021/jp1120299.

97 Y. Xu, Q. Wu, Y. Sun, H. Bai and G. Shi, *ACS Nano*, , DOI:10.1021/nn1027104.

98 N. M. N. Gomesh, A. H. Ibrahim, R. Syafinar, M. Irwanto, M. R. Mamat, Y. M Irwan, U. Hashim2, *Int. J. Ser. Eng. Sci.*, 2015, **1**, 49–65.

99 I. A. Sahito, K. C. Sun, A. A. Arbab, M. B. Qadir, Y. S. Choi and S. H. Jeong, *J. Power Sources*, , DOI:10.1016/j.jpowsour.2016.04.025.

100 H. Wang, K. Sun, F. Tao, D. J. Stacchiola and Y. H. Hu, *Angew. Chemie - Int. Ed.*, , DOI:10.1002/anie.201303497.

101 Y. S. Yen, H. H. Chou, Y. C. Chen, C. Y. Hsu and J. T. Lin, *J. Mater. Chem.*, , DOI:10.1039/c2jm30362k.

102 U. Mehmood, S. U. Rahman, K. Harrabi, I. A. Hussein and B. V. S. Reddy, *Adv. Mater. Sci. Eng.*, 2014.

103 M. Papageorgiou, N.; Maier, W. F.; Grätzel, *J. Electrochem. Soc.*, , DOI:10.1149/1.1837502.

104 N. Papageorgiou, *J. Electrochem. Soc.*, , DOI:10.1149/1.1837502.

105 S. S. Kim, S. I. Na, J. Jo, D. Y. Kim and Y. C. Nah, *Appl. Phys. Lett.*, ,

DOI:10.1063/1.2967471.

106 X. Fang, T. Ma, G. Guan, M. Akiyama, T. Kida and E. Abe, *J. Electroanal. Chem.*, , DOI:10.1016/j.jelechem.2004.04.004.

107 J. Velten, A. J. Mozer, D. Li, D. Officer, G. Wallace, R. Baughman and A. Zakhidov, *Nanotechnology*, , DOI:10.1088/0957-4484/23/8/085201.

108 H. Choi, H. Kim, S. Hwang, W. Choi and M. Jeon, in *Solar Energy Materials and Solar Cells*, 2011.

109 X. Xu, D. Huang, K. Cao, M. Wang, S. M. Zakeeruddin and M. Grätzel, *Sci. Rep.*, , DOI:10.1038/srep01489.

110 Q. Chang, Z. Ma, J. Wang, Y. Yan, W. Shi, Q. Chen, Y. Huang, Q. Yu and L. Huang, *Electrochim. Acta*, , DOI:10.1016/j.electacta.2014.11.074.

111 S. Casaluci, M. Gemmi, V. Pellegrini, A. Di Carlo and F. Bonaccorso, *Nanoscale*, 2016.

112 G. Wang, S. Zhuo and W. Xing, *Mater. Lett.*, , DOI:10.1016/j.matlet.2011.11.086.

113 D. Dodoo-Arhin, R. C. T. Howe, G. Hu, Y. Zhang, P. Hiralal, A. Bello, G. Amaratunga and T. Hasan, *Carbon N. Y.*, , DOI:10.1016/j.carbon.2016.04.012.

114 G. Yue, J. Wu, Y. Xiao, M. Huang, J. Lin, L. Fan and Z. Lan, *Electrochim. Acta*, , DOI:10.1016/j.electacta.2012.11.020.

115 A. Kaniyoor and S. Ramaprabhu, *J. Appl. Phys.*, , DOI:10.1063/1.3600231.

116 L. Kavan, J. H. Yum, M. K. Nazeeruddin and M. Grätzel, *ACS Nano*, , DOI:10.1021/nn203416d.

117 A. Kay and M. Grätzel, *Sol. Energy Mater. Sol. Cells*, , DOI:10.1016/0927-0248(96)00063-3.

118 K. Imoto, K. Takahashi, T. Yamaguchi, T. Komura, J. I. Nakamura and K. Murata, *Sol. Energy Mater. Sol. Cells*, , DOI:10.1016/S0927-0248(03)00021-7.

119 K. Suzuki, M. Yamaguchi, M. Kumagai and S. Yanagida, *Chem. Lett.*, , DOI:10.1246/cl.2003.28.

120 W. J. Lee, E. Ramasamy, D. Y. Lee and J. S. Song, *ACS Appl. Mater. Interfaces*, , DOI:10.1021/am800249k.

121 Z. Li, F. Gong, G. Zhou and Z. S. Wang, *J. Phys. Chem. C*, , DOI:10.1021/jp401032c.

122 Y. Xue, J. Liu, H. Chen, R. Wang, D. Li, J. Qu and L. Dai, *Angew. Chemie - Int. Ed.*, , DOI:10.1002/anie.201207277.

123 X. Meng, C. Yu, X. Song, Y. Liu, S. Liang, Z. Liu, C. Hao and J. Qiu, *Adv. Energy Mater.*, , DOI:10.1002/aenm.201500180.

124 M. J. Ju, J. C. Kim, H. J. Choi, I. T. Choi, S. G. Kim, K. Lim, J. Ko, J. J. Lee, I. Y. Jeon, J. B. Baek and H. K. Kim, *ACS Nano*, , DOI:10.1021/nn4009774.

125 Q. Luo, F. Hao, S. Wang, H. Shen, L. Zhao, J. Li, M. Grätzel and H. Lin, *J. Phys. Chem. C*, , DOI:10.1021/jp5004424.

126 Y. Xue, J. M. Baek, H. Chen, J. Qu and L. Dai, *Nanoscale*, , DOI:10.1039/c4nr06969b.

127 X. Cui, J. Xiao, Y. Wu, P. Du, R. Si, H. Yang, H. Tian, J. Li, W. H. Zhang, D. Deng and X. Bao, *Angew. Chemie - Int. Ed.*, , DOI:10.1002/anie.201602097.

128 B. Tang, G. Hu, H. Gao and Z. Shi, *J. Power Sources*, , DOI:10.1016/j.jpowsour.2013.01.130.

129 J. Y. Kim, J. Y. Lee, K. Y. Shin, H. Jeong, H. J. Son, C. H. Lee, J. H. Park, S. S. Lee, J. G. Son and M. J. Ko, *Appl. Catal. B Environ.*, , DOI:10.1016/j.apcatb.2016.04.008.

130 I. A. Sahito, K. C. Sun, A. A. Arbab, M. B. Qadir and S. H. Jeong, *Electrochim. Acta*, , DOI:10.1016/j.electacta.2015.05.035.

131 M. Licklederer, G. Cha, R. Hahn and P. Schmuki, *J. Electrochem. Soc.*, , DOI:10.1149/2.0031905jes.

132 D. W. Zhang, X. D. Li, H. B. Li, S. Chen, Z. Sun, X. J. Yin and S. M. Huang, *Carbon N. Y.*, , DOI:10.1016/j.carbon.2011.08.005.

133 H. Choi, H. Kim, S. Hwang, Y. Han and M. Jeon, *J. Mater. Chem.*, , DOI:10.1039/c1jm11145k.

134 W. Hong, Y. Xu, G. Lu, C. Li and G. Shi, *Electrochem. commun.*, 2008, **10**, 1555–1558.

135 K. S. Lee, Y. Lee, J. Y. Lee, J. H. Ahn and J. H. Park, *ChemSusChem*, , DOI:10.1002/cssc.201100430.

136 F. Gong, H. Wang and Z. S. Wang, *Phys. Chem. Chem. Phys.*, , DOI:10.1039/c1cp22542a.

137 M. Y. Yen, C. C. Teng, M. C. Hsiao, P. I. Liu, W. P. Chuang, C. C. M. Ma, C. K. Hsieh, M. C. Tsai and C. H. Tsai, *J. Mater. Chem.*, , DOI:10.1039/c1jm11850a.

138 Y. Y. Dou, G. R. Li, J. Song and X. P. Gao, *Phys. Chem. Chem. Phys.*, , DOI:10.1039/c2cp23775j.

139 H. Wang, K. Sun, F. Tao, D. J. Stacchiola and Y. H. Hu, *Angew. Chemie - Int. Ed.*, , DOI:10.1002/anie.201303497.

140 G. Wang, W. Xing and S. Zhuo, *Electrochim. Acta*, , DOI:10.1016/j.electacta.2013.01.034.

141 X. Fang, M. Li, K. Guo, J. Li, M. Pan, L. Bai, M. Luoshan and X. Zhao, *Electrochim. Acta*, , DOI:10.1016/j.electacta.2014.06.075.

142 X. Fang, M. Li, K. Guo, Y. Zhu, Z. Hu, X. Liu, B. Chen and X. Zhao, *Electrochim. Acta*, , DOI:10.1016/j.electacta.2012.01.038.

143 S. P. Lim, A. Pandikumar, N. M. Huang and H. N. Lim, *Int. J. Energy Res.*, , DOI:10.1002/er.3307.

144 A. C. M. San Esteban and E. P. Enriquez, *Sol. Energy*, , DOI:10.1016/j.solener.2013.09.036.

145 A. A. Al-Ghamdi, R. K. Gupta, P. K. Kahol, S. Wageh, Y. A. Al-Turki, W. El Shirbeeny and F. Yakuphanoglu, *Solid State Commun.*, , DOI:10.1016/j.ssc.2013.12.021.

146 T. H. Tsai, S. C. Chiou and S. M. Chen, *Int. J. Electrochem. Sci.*

147 J. Fan, S. Liu and J. Yu, *J. Mater. Chem.*, , DOI:10.1039/c2jm33104g.

148 A. Y. Kim, J. Kim, M. Y. Kim, S. W. Ha, N. T. T. Tien and M. Kang, *Bull. Korean Chem. Soc.*, , DOI:10.5012/bkcs.2012.33.10.3355.

149 N. Sawhney, A. Raghav and S. Satapathi, *IEEE J. Photovoltaics*, ,

DOI:10.1109/JPHOTOV.2016.2639343.

150 G. Richhariya, A. Kumar, P. Tekasakul and B. Gupta, *Renew. Sustain. Energy Rev.*, 2017.

151 N. T. R. N. Kumara, A. Lim, C. M. Lim, M. I. Petra and P. Ekanayake, *Renew. Sustain. Energy Rev.*, 2017.

152 W. Stahl and H. Sies, *Mol. Aspects Med.*, 2003.

153 X. F. Wang, R. Fujii, S. Ito, Y. Koyama, Y. Yamano, M. Ito, T. Kitamura and S. Yanagida, *Chem. Phys. Lett.*, , DOI:10.1016/j.cplett.2005.09.020.

154 X. F. Wang, Y. Koyama, H. Nagae, Y. Yamano, M. Ito and Y. Wada, *Chem. Phys. Lett.*, , DOI:10.1016/j.cplett.2006.01.003.

155 X. F. Wang, A. Matsuda, Y. Koyama, H. Nagae, S. ichi Sasaki, H. Tamiaki and Y. Wada, *Chem. Phys. Lett.*, , DOI:10.1016/j.cplett.2006.04.008.

156 M. Grätzel, *J. Photochem. Photobiol. A Chem.*, , DOI:10.1016/j.jphotochem.2004.02.023.

157 H. Zhou, L. Wu, Y. Gao and T. Ma, *J. Photochem. Photobiol. A Chem.*, , DOI:10.1016/j.jphotochem.2011.02.008.

158 G. Calogero, J. H. Yum, A. Sinopoli, G. Di Marco, M. Grätzel and M. K. Nazeeruddin, *Sol. Energy*, , DOI:10.1016/j.solener.2012.02.018.

159 S. Hao, J. Wu, Y. Huang and J. Lin, in *Solar Energy*, 2006.

160 W. Wu, J. Hua, Y. Jin, W. Zhan and H. Tian, *Photochem. Photobiol. Sci.*, , DOI:10.1039/b712439b.

161 X. Ma, J. Hua, W. Wu, Y. Jin, F. Meng, W. Zhan and H. Tian, *Tetrahedron*, ,

DOI:10.1016/j.tet.2007.10.094.

162 K. Hara, M. Kurashige, Y. Dan-Oh, C. Kasada, A. Shinpo, S. Suga, K. Sayama and H. Arakawa, *New J. Chem.*, , DOI:10.1039/b300694h.

163 Z. S. Wang, Y. Cui, K. Hara, Y. Dan-Oh, C. Kasada and A. Shinpo, *Adv. Mater.*, , DOI:10.1002/adma.200601020.

164 H. N. Tsao, J. Burschka, C. Yi, F. Kessler, M. K. Nazeeruddin and M. Grätzel, *Energy Environ. Sci.*, , DOI:10.1039/c1ee02389f.

165 B. P. Jelle, C. Breivik and H. Drolsum Røkenes, *Sol. Energy Mater. Sol. Cells*, , DOI:10.1016/j.solmat.2011.12.016.

166 L. P. Heiniger, P. G. O'Brien, N. Soheilnia, Y. Yang, N. P. Kherani, M. Grätzel, G. A. Ozin and N. Tétreault, *Adv. Mater.*, , DOI:10.1002/adma.201302113.

167 F. Zanjanchi and J. Beheshtian, *J. Iran. Chem. Soc.*, , DOI:10.1007/s13738-018-1561-2.

168 A. K. Pandey, M. S. Ahmad, N. A. Rahim, V. V. Tyagi and R. Saidur, in *Environmental Biotechnology: For Sustainable Future*, 2018.

169 G. R. A. Kumara, S. Kaneko, M. Okuya, B. Onwona-Agyeman, A. Konno and K. Tennakone, *Sol. Energy Mater. Sol. Cells*, , DOI:10.1016/j.solmat.2005.07.007.

170 M. Z. Iqbal, S. R. Ali and S. Khan, *Sol. Energy*, 2019.

171 W. Ghann, H. Kang, T. Sheikh, S. Yadav, T. Chavez-Gil, F. Nesbitt and J. Uddin, *Sci. Rep.*, , DOI:10.1038/srep41470.

172 P. Sanjay, K. Deepa, J. Madhavan and S. Senthil, *Mater. Lett.*, ,

910 DOI:10.1016/j.matlet.2018.02.085.

911 173 G. Calogero, A. Bartolotta, G. Di Marco, A. Di Carlo and F. Bonaccorso, *Chem.*
912 *Soc. Rev.*, , DOI:10.1039/c4cs00309h.

913 174 N. M. Gómez-Ortíz, I. A. Vázquez-Maldonado, A. R. Pérez-Espadas, G. J.
914 Mena-Rejón, J. A. Azamar-Barrios and G. Oskam, *Sol. Energy Mater. Sol.*
915 *Cells*, , DOI:10.1016/j.solmat.2009.05.013.

916 175 X. F. Wang, C. H. Zhan, T. Maoka, Y. Wada and Y. Koyama, *Chem. Phys.*
917 *Lett.*, , DOI:10.1016/j.cplett.2007.08.097.

918 176 A. R. Glenn, *Annu. Rev. Microbiol.*, 1976, **30**, 41–62.

919 177 Ribosome, https://www.nature.com/scitable/definition/ribosome-194.

920 178 Ribosomes, Transcription, and Translation,
921 https://www.nature.com/scitable/topicpage/ribosomes-transcription-and-
922 translation-14120660.

923 179 G. K. Chandi and B. S. Gill, *Int. J. Food Prop.*, ,
924 DOI:10.1080/10942910903256956.

925 180 J.-L. Barredo, *Microbial Carotenoids from Bacteria and Microalgae. Methods*
926 *and Protocols*, 2012.

927 181 K. Kirti, S. Amita, S. Priti, A. Mukesh Kumar and S. Jyoti, *Adv. Biol.*, ,
928 DOI:10.1155/2014/837891.

929 182 X. F. Wang, J. Xiang, P. Wang, Y. Koyama, S. Yanagida, Y. Wada, K.
930 Hamada, S. I. Sasaki and H. Tamiaki, *Chem. Phys. Lett.*, ,
931 DOI:10.1016/j.cplett.2005.04.067.

183 Y. Lu, M. Yuan, Y. Liu, B. Tu, C. Xu, B. Liu, D. Zhao and J. Kong, *Langmuir*, , DOI:10.1021/la0470129.

184 J. H. Caufield, M. Abreu, C. Wimble and P. Uetz, *PLoS Comput. Biol.*, , DOI:10.1371/journal.pcbi.1004107.

185 D. A. Bryant, A. M. Garcia Costas, J. A. Maresca, A. G. M. Chew, C. G. Klatt, M. M. Bateson, L. J. Tallon, J. Hostetler, W. C. Nelson, J. F. Heidelberg and D. M. Ward, *Science (80-.).*, , DOI:10.1126/science.1143236.

186 Q. Fu, C. Zhao, S. Yang and J. Wu, *Mater. Lett.*, , DOI:10.1016/j.matlet.2014.05.054.

187 A. Mishra, M. K. Fischer and P. Bauerle, *Angew Chem Int Ed Engl*, , DOI:10.1002/anie.200804709.

188 Y. Cui, Y. Wu, X. Lu, X. Zhang, G. Zhou, F. B. Miapeh, W. Zhu and Z. S. Wang, *Chem. Mater.*, , DOI:10.1021/cm202226j.

189 A. Kay and M. Graetzel, *J. Phys. Chem.*, , DOI:10.1021/j100125a029.

190 S. Ahmad, E. Guillén, L. Kavan, M. Grätzel and M. K. Nazeeruddin, *Energy Environ. Sci.*, 2013.

191 G. B. Ferreira, E. Hollauer, N. M. Comerlato and J. L. Wardell, *Spectrochim. Acta - Part A Mol. Biomol. Spectrosc.*, , DOI:10.1016/j.saa.2007.12.010.

192 C. N. Ramachandran, D. Roy and N. Sathyamurthy, *Chem. Phys. Lett.*, , DOI:10.1016/j.cplett.2008.06.073.

193 G. Calogero, A. Sinopoli, I. Citro, G. Di Marco, V. Petrov, A. M. Diniz, A. J. Parola and F. Pina, *Photochem. Photobiol. Sci.*, , DOI:10.1039/c3pp25347c.

194 T. Ruiz-Anchondo, N. Flores-Holguín and D. Glossman-Mitnik, *Molecules*, , DOI:10.3390/molecules15074490.

195 J. B. L. Martins, J. A. Durães, M. J. A. Sales, A. S. F. A. Vilela, G. M. E. Silva and R. Gargano, *Int. J. Quantum Chem.*, , DOI:10.1002/qua.21845.

196 X. F. Wang, H. Tamiaki, O. Kitao, T. Ikeuchi and S. I. Sasaki, *J. Power Sources*, , DOI:10.1016/j.jpowsour.2013.05.191.

197 F. A. Castro, A. Faes, T. Geiger, C. F. O. Graeff, M. Nagel, F. Nüesch and R. Hany, *Synth. Met.*, , DOI:10.1016/j.synthmet.2006.06.010.

198 Y.-S. Kim, J.-I. Shin, S.-Y. Park, K. Jun and Y.-A. Son, *Text. Color. Finish.*, , DOI:10.5764/tcf.2009.21.5.035.

199 K. Liu, Y. Yao, J. Wang, L. Zhu, M. Sun, B. Ren, L. Xie, Y. Luo, Q. Meng and X. Zhan, *Mater. Chem. Front.*, , DOI:10.1039/c6qm00097e.

200 Y. Qian, Y. Ni, S. Yue, W. Li, S. Chen, Z. Zhang, L. Xie, M. Sun, Y. Zhao and W. Huang, *RSC Adv.*, , DOI:10.1039/c5ra00694e.

201 B. B. Carbas and A. M. Önal, *Electrochim. Acta*, , DOI:10.1016/j.electacta.2012.01.026.

202 R. Sánchez-De-Armas, M. Á. San Miguel, J. Oviedo and J. F. Sanz, *Phys. Chem. Chem. Phys.*, , DOI:10.1039/c1cp22058f.

203 J. M. D. Agrawal, S., Dev, P., English, N. J., Thampi, K. R., & MacElroy, *J. Mater. Chem.*, 2011, **21**, 11101–11108.

204 K. Nagai, A., & Takagi, *Conjugated Objects: Developments, Synthesis, and Applications*, Pan Stanford, 2017.

205 G. N. Lewis and M. Calvin, *Chem. Rev.*, , DOI:10.1021/cr60081a004.

206 Samal, A Brief Discussion on Color: Why does such conjugation allow absorption of visible light?, https://people.chem.umass.edu/samal/269/color.pdf.

207 R. J. Franck, H., & Cogdell, in *A. Young, G. Britton eds. Carotenoids in Photosynthesis.*, 1993.

208 R. Koyama, Y., & Fujii, in *The photochemistry of carotenoids*, Springer, Dordrecht, 1999, pp. 161–188.

209 H. A. Frank and G. W. Brudvig, *Biochemistry*, 2004.

210 D. Yu, G. Zhu, S. Liu, B. Ge and F. Huang, *Int. J. Hydrogen Energy*, , DOI:10.1016/j.ijhydene.2013.02.114.

211 M. F. Montagni, T., Enciso, P., Marizcurrena, J. J., Castro-Sowinski, S., Fontana, C., Davyt, D., & Cerdá, *Environ. Sustain.*, 2018, 1–9.

212 S. K. Srivastava, P. Piwek, S. R. Ayakar, A. Bonakdarpour, D. P. Wilkinson and V. G. Yadav, *Small*, , DOI:10.1002/smll.201800729.

213 A. Mershin, K. Matsumoto, L. Kaiser, D. Yu, M. Vaughn, M. K. Nazeeruddin, B. D. Bruce, M. Graetzel and S. Zhang, *Sci. Rep.*, , DOI:10.1038/srep00234.

214 J. Chellamuthu, P. Nagaraj, S. G. Chidambaram, A. Sambandam and A. Muthupandian, *J. Photochem. Photobiol. B Biol.*, , DOI:10.1016/j.jphotobiol.2016.06.044.